JCB Journal of Cell Biology

ARTICLE

Rie1 and Sgn1 form an RNA-binding complex that enforces the meiotic entry cell fate decision

Alec Gaspary[1], Raphaelle Laureau[1], Annie Dyatel[1], Gizem Dursuk[1], Yael Simon[1], and Luke E. Berchowitz[1,2]

Budding yeast cells have the capacity to adopt few but distinct physiological states depending on environmental conditions. Vegetative cells proliferate rapidly by budding while spores can survive prolonged periods of nutrient deprivation and/or desiccation. Whether or not a yeast cell will enter meiosis and sporulate represents a critical decision that could be lethal if made in error. Most cell fate decisions, including those of yeast, are understood as being triggered by the activation of master transcription factors. However, mechanisms that enforce cell fates posttranscriptionally have been more difficult to attain. Here, we perform a forward genetic screen to determine RNA-binding proteins that affect meiotic entry at the posttranscriptional level. Our screen revealed several candidates with meiotic entry phenotypes, the most significant being *RIE1*, which encodes an RRM-containing protein. We demonstrate that Rie1 binds RNA, is associated with the translational machinery, and acts posttranscriptionally to enhance protein levels of the master transcription factor Ime1 in sporulation conditions. We also identified a physical binding partner of Rie1, Sgn1, which is another RRM-containing protein that plays a role in timely Ime1 expression. We demonstrate that these proteins act independently of cell size regulation pathways to promote meiotic entry. We propose a model explaining how constitutively expressed RNA-binding proteins, such as Rie1 and Sgn1, can act in cell fate decisions both as switch-like enforcers and as repressors of spurious cell fate activation.

Introduction

Both eukaryotic and prokaryotic cells make developmental fate decisions based on an array of environmental and developmental cues. The cell must sense, accurately process, and, in some cases, quantify multiple cues to adopt the proper physiological state (Furlong, 2010; Kilian et al., 2010). Multicellular eukaryotes rely on cell fate commitment through several pathways to create the diverse cell types needed for proper organismal development (Guo et al., 2010; Hetz, 2012; Dalton, 2015). These pathways are often irreversible and involve a discrete commitment point where the cell chooses a distinct developmental fate (Cappell et al., 2016). Analogous cell fate decisions also occur in unicellular eukaryotes (Tsuchiya et al., 2014).

The budding yeast *Saccharomyces cerevisiae* undergoes a few well-defined cell fate decisions during its life cycle, making it an advantageous model to study the mechanisms that commit a cell to a particular fate (Herskowitz, 1988). A yeast cell in G1 can choose to remain in G1, continue vegetative growth by budding, transition to filamentous growth, enter sexual conjugation, or commit to the meiotic developmental process that occurs in the context of sporulation (Hartwell, 1974). During meiosis, one diploid yeast cell becomes four haploid gamete spores. Each cell fate carries strengths and drawbacks—budding cells can proliferate rapidly in nutrient-rich conditions while spores can survive long periods of desiccation and or nutrient deprivation. The control of meiotic entry in yeast is a complex system in which several biological pathways are involved such as sensing glucose and nitrogen, cell size, and cell-cycle progression (Honigberg and Purnapatre, 2003; van Werven and Amon, 2011). The decision of whether to initiate meiosis and enter sporulation is crucial to maintaining fitness and, if triggered in error, can be lethal (Mitchell and Bowdish, 1992).

The expression of the master regulatory transcription factor Ime1 is a key event leading to commitment to meiotic entry, and its expression is tightly controlled (Kassir et al., 1988; Smith et al., 1990). In addition to its roles as a direct transcriptional activator of early meiotic genes, Ime1 drives degradation of the Ume6 repressor, which allows robust expression of several key early meiotic transcripts (Mallory et al., 2007). The *IME1* promoter contains multiple regulatory sites that integrate cell-intrinsic and environmental signals, including ploidy and nutrient availability (Kahana et al., 2010; van Werven and Amon, 2011; Tam and van Werven, 2020). While the transcriptional requirements for

[1]Department of Genetics and Development, Hammer Health Sciences Center, Columbia University Irving Medical Center, New York, NY, USA; [2]Taub Institute for Research on Alzheimer's and the Aging Brain, New York, NY, USA.

Correspondence to Luke E. Berchowitz: leb2210@cumc.columbia.edu.

meiotic entry in yeast are well-defined, how posttranscriptional mechanisms, which are critical for proper meiotic progression (Sherman et al., 1993; Brar et al., 2012; Kim and Strich, 2016), influence the meiotic cell fate decision are less understood.

RNA-binding proteins (RBPs) are crucial for posttranscriptional regulation and affect numerous biological processes, including gametogenesis (Glisovic et al., 2008). RNA-binding proteins can modify all steps of the mRNA life cycle including transcription, processing (splicing, polyadenylation, etc.), export/localization, translation, and degradation (Dreyfuss et al., 2002). Some RBPs have been identified in budding yeast as essential posttranscriptional regulators of gametogenesis such as Rim4, an RNA recognition motif (RRM)–containing RBP, which controls the translation of several middle-stage meiosis genes (Soushko and Mitchell, 2000; Deng and Saunders, 2001; Berchowitz et al., 2013). Additionally, some members of the *WHI* family encode RBPs that influence meiotic cell fate by posttranscriptionally regulating genes that control cell size (Garí et al., 2001; Day et al., 2004).

We hypothesized that there may be unknown yeast RBPs that are inessential for vegetative growth but critical for meiosis. Here, we identify two such RBPs, Rie1 and Sgn1, which form a complex that is required for the timely entry into meiosis and thus the spore cell fate. We show that Rie1 and Sgn1 act posttranscriptionally to promote Ime1 expression and timely entry into premeiotic DNA synthesis. We show through targeted mutations that the RNA-binding domains of Rie1 are necessary for its role in meiotic entry. We also demonstrate that Rie1 and Sgn1 act through a pathway independent of cell size control or poly(A) tail length. Our results support a model in which Rie1 and Sgn1 act directly to promote meiotic entry as switch-like enforcers while also playing an indirect role to repress spurious meiotic entry.

Results

A forward genetic screen reveals *RIE1* as an important meiotic entry factor

We performed a systematic screen in the efficient sporulation strain SK1 (Kane and Roth, 1974) to identify RBPs that are important for meiotic entry in *S. cerevisiae* (Fig 1 A). We generated a library of diploid strains, each homozygous for a meiotic entry reporter construct and a single deletion of a gene encoding a putative RBP. We used Zip1-GFP as a readout for meiotic entry because it is expressed, and localized to the nucleus, specifically during meiotic prophase I. Strains also harbored *ndt80Δ* (Xu et al., 1995) to prevent exit from pachynema and loss of Zip1-GFP signal. Putative RBPs were defined as harboring one or more of the following annotated domains: RRMs, K Homology domains, retrotransposon-like zinc knuckle CCHC domains, zinc finger CCCH-type, Pumilio Family domains, double-stranded RNA binding domains, and pentatricopeptide repeat domains (Finn et al., 2014; Fig S1 A and Table S1). After excluding petite mutants, which do not enter meiosis (Ephrussi and Hottinguer, 1951), and essential genes, we were left with 64 mutant strains from an original pool of 103.

Strains were sporulated in liquid culture and samples were taken at 0 and 6 h for analysis by fluorescence microscopy. We quantified the percentage of Zip1-positive cells at 6 h in three biological replicates (Fig. 1 B). We grouped RBP mutants into three categories based on natural breakpoints in the data: no meiotic defect (>75% Zip1+, 39), mild meiotic entry defect (45–75%, 17), and severe meiotic entry defect (<45%, 8). The most severe entry mutant we observed was *rie1Δ*, which showed ~15% of cells entering meiotic prophase at 6 h (Fig. 1, B and C). By live cell imaging of *rie1Δ* and wild type, we confirmed that *rie1Δ* cells exhibit a severe meiotic entry defect—after 15 h, on average, 59% of wild type and 10% of *rie1Δ* cells entered meiosis (Fig. 1 D; Video 1; and Video 2). Of the cells that entered meiosis, we found that onset of metaphase I in *rie1Δ* cells was, on average, 162 min later than wild type cells (Fig. 1 E). Furthermore, metaphase I, metaphase II, and anaphase II were all significantly slowed (2.1-, 1.9-, and 1.5-fold longer, respectively) in *rie1Δ* cells compared with wild type (Fig. 1 F). Anaphase I length was indistinguishable between wild type and *rie1Δ*. These results support the notion that Rie1 may also be important for progression through the meiotic divisions in addition to its role in promoting meiotic entry.

rie1Δ mutants do not properly accumulate Ime1 in conditions promoting sporulation

RIE1 (also called *WHI8*) encodes a protein harboring three predicted RRMs and three intrinsically disordered regions (Fig. 2 A). Each of the RRMs contains an RNP1 and RNP2 motif with phenylalanine residues that are essential for nucleic acid-binding function (Maris et al., 2005). We confirmed that Rie1 binds RNA and that point mutation of RNP motifs within RRM2 and RRM3 affected RNA binding capacity (Fig. S1 B). All three RRM mutants exhibited decreased steady-state abundance (RRM1 and RRM3 mutants being more severe), suggesting that functional RRMs are important for Rie1 stability (Fig. S1 C). We found that Rie1 is expressed in both mitotic and meiotic cells, and its abundance increases approximately threefold after overnight growth in acetate-containing presporulation medium (Fig. S1 D). Using a Rie1-Envy GFP fusion (Slubowski et al., 2015), we observed that during meiosis, Rie1 is mainly cytoplasmic with both diffuse and granular morphology (Fig. S1 E). Because *RIE1* was reported to regulate cell size in mitosis (Yahya et al., 2021), we tested whether *rie1Δ* mutants exhibit mitotic growth defects. We found that (in the SK1 strain background) the mitotic growth of *rie1Δ* mutants did not significantly differ from wild type in four media conditions (YPD complex–rich media, SDC semi-defined media, BYTA presporulation acetate-containing media, and YPG glycerol-containing non-fermentable media, Fig. 2 B). Our results indicate that the severe *rie1Δ* phenotype, under the conditions we tested, is specific to meiosis.

Because *rie1Δ* mutants do not properly enter meiotic prophase I and exhibit no growth defect in presporulation medium, we hypothesized that they fail to express a factor that promotes meiotic entry. To test this idea, we compared the mRNA and protein levels (using C-terminal epitope tags) of three key inducer of meiosis (Ime) factors, Ime1, Ime2, and Ime4, in diploid

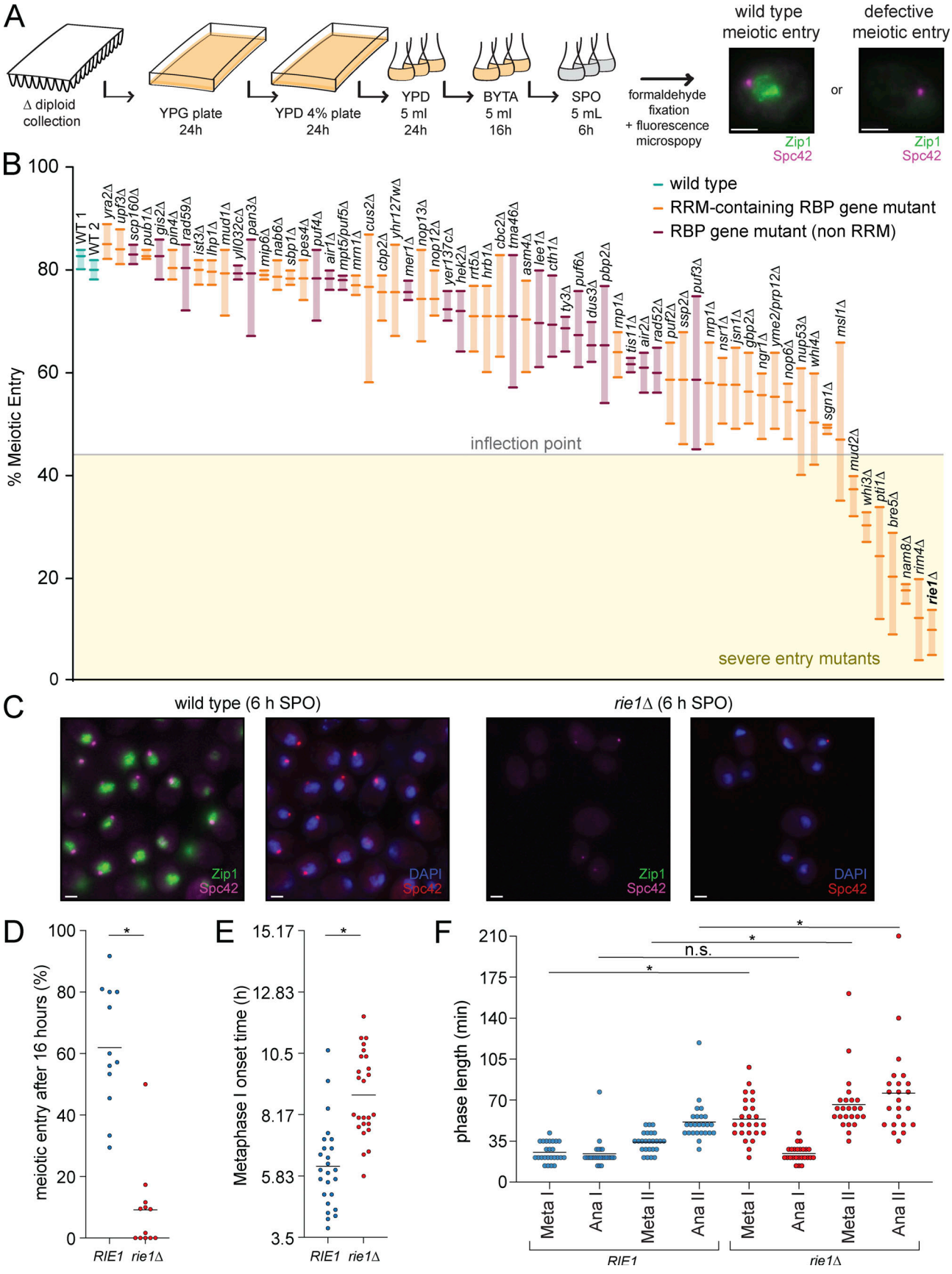

Figure 1. **A forward genetic screen for meiotic mutants reveals *RIE1* as an entry factor. (A)** Schematic overview of RBP meiotic entry screen. Representative fluorescence images are shown for wild type (B2381) and a meiotic entry mutant (*rim4Δ*, B2585). Zip1-GFP is shown in green, Spc42-mCherry is

shown in magenta. Scale bar, 2 µm. **(B)** Strains homozygous for Zip1-GFP, Spc42-mCherry, *ndt80Δ*, and deletion of a gene encoding an RBP-containing protein were induced to sporulate at 30°C. At 6 h, when cells had arrested in G2 due to the lack of *NDT80*, cells were collected, fixed with formaldehyde, and nuclear Zip1 signal was assessed by fluorescence microscopy with DAPI staining to assess position of the nucleus. The y axis shows the percentage of Zip1-positive cells as defined by a fivefold nuclear GFP signal over the background. Shown are screen results of three biological replicates where each point represents an independent experiment. Orange bars indicate RRM mutants, and purple bars indicate genes encoding RBPs without an RRM. The results of two wild type control strains (B2381) are shown in teal. **(C)** *rie1Δ* mutants exhibit a severe entry phenotype. Shown are representative examples of images taken at 6 h for wild type (B2381) and *rie1Δ* (B2397) cells. Zip1-GFP is shown in green, Spc42-mCherry is shown in magenta (left panels) or red (right panels), and DAPI in blue. Scale bar, 2 µm. **(D–F)** Strains harboring fluorescently labeled tubulin (*pTUB1-GFP-TUB1*) and Spc42 (*SPC42-mCherry*) and either *RIE1* (wild type, B1451) or *rie1Δ* (B1514) were induced to sporulate at 30°C. After 2.5 h of growth, the cells were loaded onto a microfluidics chip (Cell Asic), points were established, and cells were imaged every 7 min starting at 3.5 h. **(D)** Percentage of cells entering meiosis was recorded. Each point represents the percentage entry in a field of view (n = 12 fields [minimum five cells] for each genotype). **(E and F)** Single-cell analysis (for cells that entered meiosis, n = 25 for each genotype) of (E) time of metaphase I onset and (F) time in metaphase I, anaphase I, metaphase II, and anaphase II. Mean is indicated by a black bar and statistical significance (*P < 0.05) was determined by a two-sided student's t test (data distribution was tested for normality).

rie1Δ and wild type cells upon transfer to sporulation (SPO) medium (Fig. 2, C and D; and Fig. S2 A). The prominence of Ime1 is discussed above, Ime2 is a cyclin-dependent kinase-like kinase (Guttmann-Raviv et al., 2002), and Ime4 is an mRNA N6-adenosine methyltransferase (Clancy et al., 2002; Hongay et al., 2006). We found that Ime1, Ime2, and Ime4 protein levels were all decreased in *rie1Δ*. Furthermore, we found that point mutation in any of the *RIE1* RRMs was similar to *rie1Δ* in that Ime1 expression was delayed but not totally abolished (Fig. 2, C and D). Because RRM mutations negatively affect Rie1 abundance, phenotypes in these strains likely reflect a combination of decreased Rie1 RNA binding as well as protein levels. As Ime1 is upstream and influences expression of *IME2* (Mitchell et al., 1990) and *IME4* is dispensable for meiosis in the SK1 strain (Groth et al., 2010), we focused on understanding how *RIE1* promotes Ime1 expression. Notably, the decreased Ime1 protein levels in *rie1* mutants did not appear to be simply a function of lower *IME1* transcript levels (Fig. 2, C and D). To assess whether Rie1 has the capacity to bind *IME1* mRNA, we conducted an electrophoretic mobility shift assay (EMSA) using in vitro transcribed *IME1* mRNA and recombinant Rie1 purified from *Escherichia coli* (Fig. S2 B). We found that Rie1 binds *IME1* mRNA compared with a control protein, bovine serum albumin (BSA), which does not bind (Fig. S2 C). Based on these data, we hypothesized that Rie1 acts as a posttranscriptional activator of *IME1*.

Because C-terminal tagging inhibits Ime1 function, we used an N-terminal super-folder GFP Ime1 fusion (sfGFP-Ime1) to further assess Ime1 expression and localization in *rie1* mutants. In these strains, expression of *sfGFP-IME1* is driven by the *IME1* promoter from its endogenous locus (Tam and van Werven, 2020). We confirmed that Ime1 protein levels (corrected for mRNA level) were decreased in *rie1Δ* cells and *rie1* RRM mutants (Fig. S3, A and B). As expected, full deletion or point mutation of *RIE1* RRMs negatively affected the nuclear abundance of Ime1 as a consequence of decreased total Ime1 levels (Fig. 2 E and Fig. S3 C). We also measured how deletion or point mutation of *RIE1* affects progression through the meiotic divisions. While *rie1Δ* had the most severe progression defect, every *rie1* RRM point mutant showed meiotic progression defects with *rie1-F604L* (RRM3) being the most severe and *rie1-F298L* (RRM2) being the least severe (Fig. 2 F). Taken together, these results support the hypothesis that the RRM domains of Rie1 are important for its function in proper Ime1 accumulation and meiotic progression.

While early meiosis events are altered in the absence of Rie1, we wanted to further examine whether *RIE1* is involved in later meiotic events. To probe this question, we created strains where Rie1 is fused with an auxin-inducible degron (AID) tag in the *NDT80-IN* block-release synchronization background, in which cells are released from a G2 arrest by the induction of *NDT80*. (Benjamin et al., 2003; Carlile and Amon, 2008). The AID tag allows for specific depletion of a protein when auxin is added to the growth medium (Nishimura et al., 2009). Using this system, we depleted Rie1 after 5 h in SPO medium and then released the cells from G2 arrest at 6 h. This allowed us to address whether Rie1 effects meiotic processes after expression of Ime1. We found that after depleting Rie1, meiotic progression was delayed as assessed by accumulation of a protein specific to the second meiotic division (Clb3) and by DAPI (Fig. 2 G). Two caveats to these experiments are that the *pRIM4-OsTIR* (auxin-inducible E3 driven by the *RIM4* promoter) and the *RIE1-AID* tag (in the absence of auxin) both negatively influence meiotic progression. Based on these data and our observations that *rie1Δ* cells show delays in metaphase I, metaphase II, and anaphase II (Fig. 1 F), we propose that Rie1 is important for later meiotic events in addition to its role as an activator of early meiosis.

The meiotic activation role of Rie1 is independent of cell size regulation

A previous study reported that Rie1 translationally represses the G1 cyclin *CLN3*, and de-repression of *CLN3* in *rie1Δ* mutants leads to decreased cell budding volume compared with wild type (Yahya et al., 2021). Because Cln3 expression negatively impacts Ime1 expression and thus meiotic entry (Garí et al., 2001; Purnapatre et al., 2002), we wanted to determine whether and to what degree *rie1Δ* phenotypes could be attributed to *CLN3* de-repression. If this is the case, the *rie1Δ* meiotic entry defect should be suppressed in a *cln3Δ* background. To assess this possibility, we compared meiotic entry and progression in wild type, *rie1Δ*, *cln3Δ*, and *rie1Δ cln3Δ* double mutants by FACS and DAPI staining. As expected, *rie1Δ* showed abnormal meiotic progression and *cln3Δ* showed efficient entry as the checkpoint for cell size entry into meiosis was made less stringent (Nachman et al., 2007). Importantly, we found that the *rie1Δ cln3Δ* double mutant did not rescue the *rie1Δ* meiotic entry defect (Fig. 3, A and B). To determine whether Rie1 influences the size of starved cells in G1 arrest (i.e., premeiotic cells), we measured

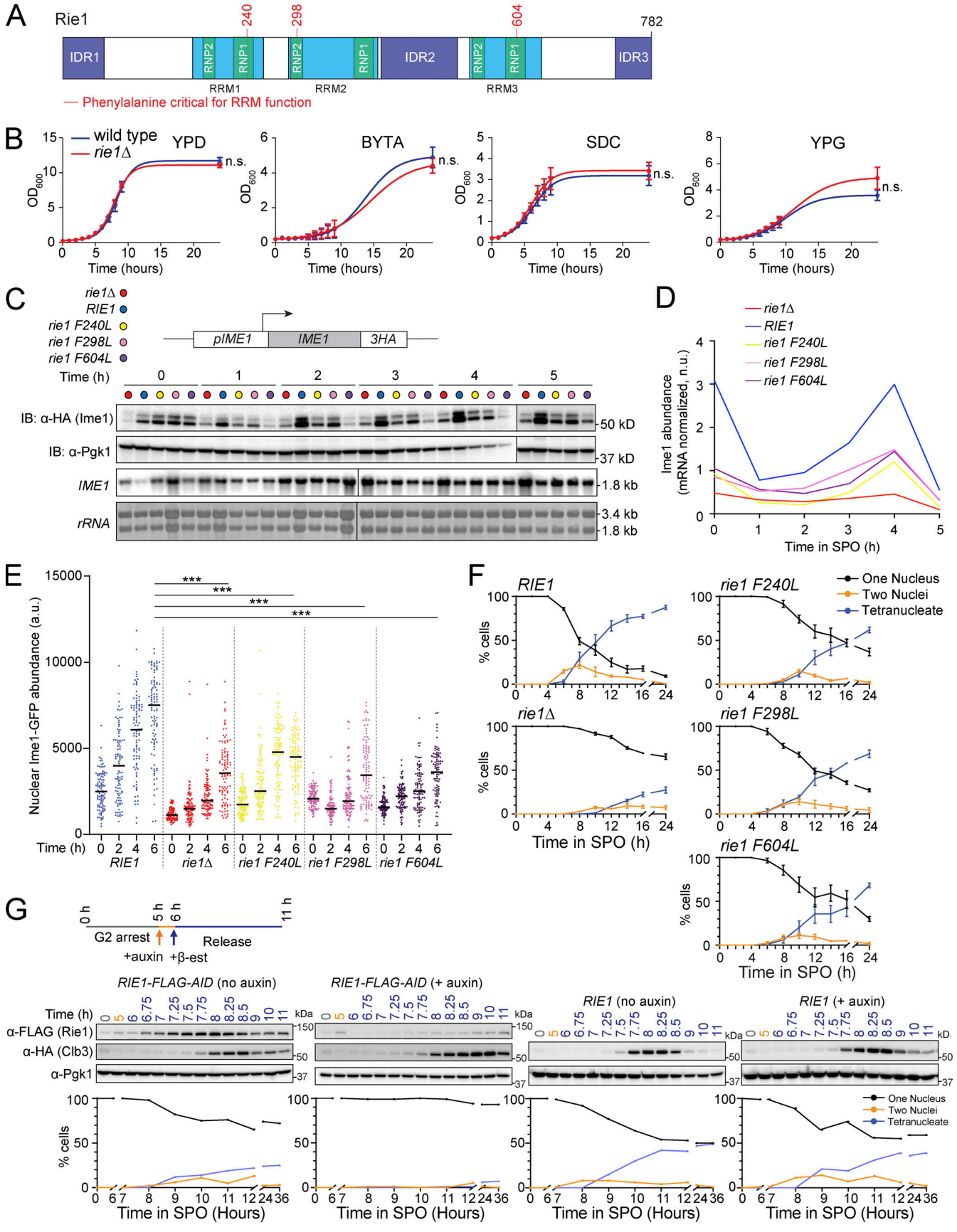

Figure 2. **Rie1 is important for Ime1 expression in early meiosis. (A)** Diagram of Rie1. RRM domains are shown in blue, RNP motifs in green, and IDRs in purple. Phenylalanine residues critical for RRM function that we subsequently mutated are indicated in red. **(B)** Vegetative growth in various media conditions

was determined in diploid wild type (B47, blue) and *rie1Δ* (B1574, red) strains. Strains were inoculated in YPD and grown overnight and then diluted to 0.2 OD_{600} the next day in YPD (glucose), BYTA (acetate) SDC (complete synthetic medium with glucose), or YPG (glycerol). Shown are mean values from three biological replicates. Statistical significance was determined by Mann–Whitney test (n.s. = not significant). **(C and D)** Strains harboring *IME1-3HA* and *rie1Δ* (B1653, red), wild type *RIE1* (B1662, blue), *rie1-F240L* (B2403, yellow), *rie1-F298L* (B2836, pink), and *rie1-F604L* (B2298, purple) were induced to sporulate at 30°C. **(C)** Protein levels of Ime1 and Pgk1 (loading) were determined by immunoblot (IB) and mRNA levels of *IME1* and *rRNA* (loading) were determined by Northern blot. **(D)** Quantification of C showing Ime1 protein abundance corrected for *IME1* mRNA levels. Biological replicates = 7. **(E and F)** Strains harboring N-terminal sfGFP-tagged (*sfGFP-IME1*) and *rie1Δ* (B1653, red), wild type *RIE1* (B1662, blue), *rie1-F240L* (B2403, yellow), *rie1-F298L* (B2836, pink), and *rie1-F604L* (B2298, purple) were induced to sporulate at 30°C. **(E)** Single-cell measurements of nuclear sfGFP-Ime1 were determined using fluorescence microscopy. Shown are individual measurements for 50 cells for each time point in each genetic background. Mean is indicated by a black bar and statistical significance (***P < 0.0001) was determined by two-sided student's *t* test with Welch's correction for SD differences. **(F)** Progression through the meiotic divisions was determined at the indicated times by DAPI staining. Biological replicates = 3 and error bars indicate SEM. **(G)** Strains harboring *NDT80-IN*, *CLB3-3HA*, *pRim4-OsTIR1*, and either *RIE1-6FLAG-AID* (B1503) or wild type *RIE1* (B1604) were induced to sporulate at 30°C. Cells were treated with auxin at 5 h (or vehicle control), released from G2-arrest at 6 h, and samples were collected at the indicated times. Protein levels of Rie1, Clb3, and Pgk1 were determined by immunoblot, and meiotic progression was determined by DAPI staining. Biological replicates = 3. Source data are available for this figure: SourceData F2.

the cell size of *rie1Δ*, *cln3Δ*, and wild type cells grown overnight in acetate growth medium (BYTA). As expected, both *cln3Δ* and *rie1Δ cln3Δ* double mutants exhibited a significantly larger cell volume than wild type cells (Fig. 3 C). We found that, in pre-meiotic conditions, the size of *rie1Δ* cells does not differ significantly from wild type, indicating that the reported smaller size of *rie1Δ* (Yahya et al., 2021) is likely limited to the context of vegetative growth. Taken together, our results indicate that the meiotic entry defect in *rie1Δ* cells is not a result of *CLN3* de-repression.

Global translation is disrupted in cells lacking *RIE1*

Because the decreased Ime1 expression in *rie1Δ* cells cannot be explained solely by decreased *IME1* mRNA levels, we hypothesized that *RIE1* encodes a translational activator. This led us to ask if *rie1Δ* cells show altered translation at a global level. To test

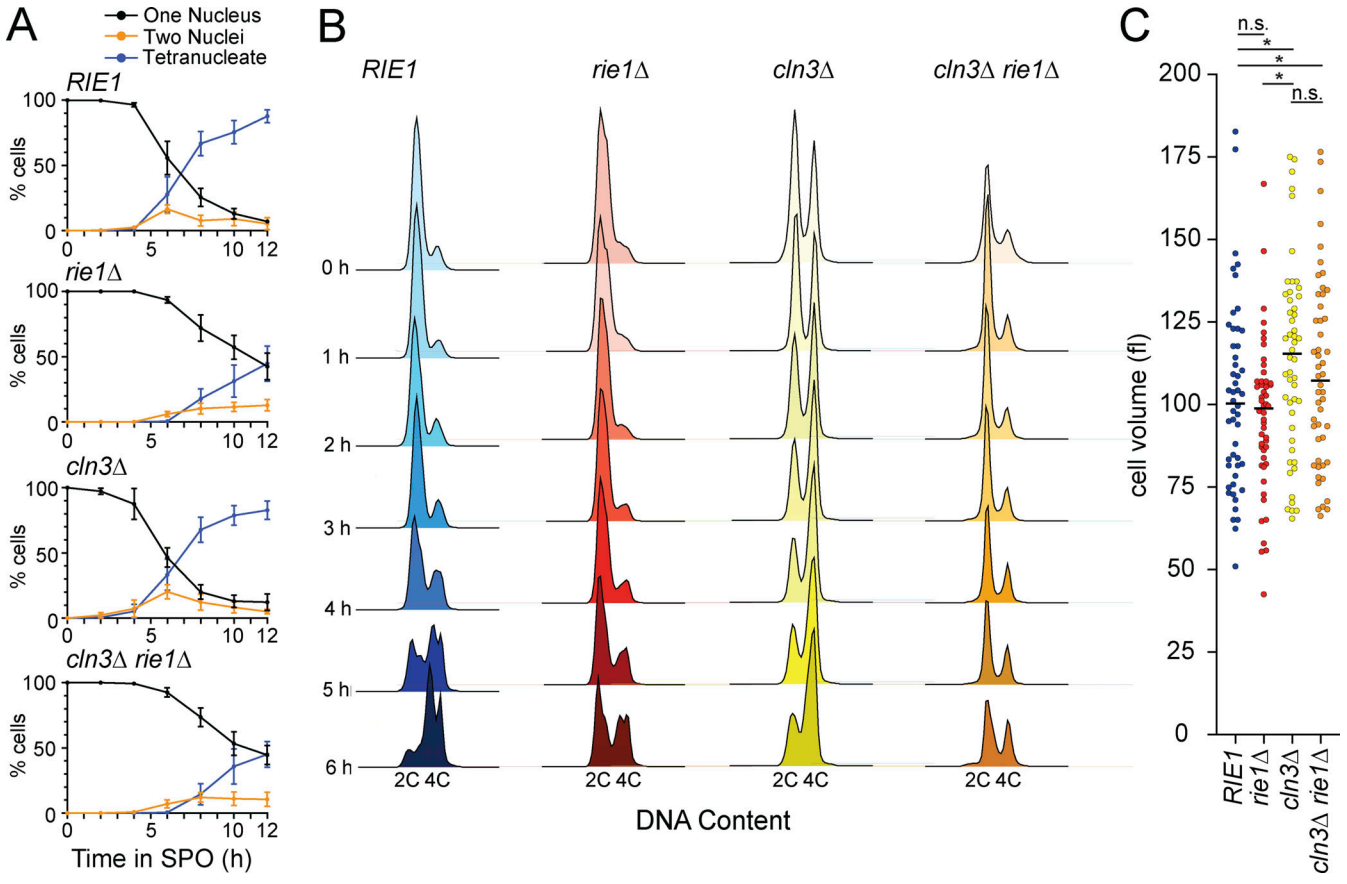

Figure 3. **Rie1 acts independently of the *CLN3* pathway to promote meiotic entry. (A and B)** Wild type (B47, blue), *rie1Δ* (B1574, red), *cln3Δ* (B2729, yellow), and *rie1Δ cln3Δ* (B2726, orange) strains were induced to sporulate at 30°C. Progression through the meiotic divisions was determined at the indicated times by DAPI staining (A) and progression through pre-meiotic S-phase by flow cytometry (B). Biological replicates = 3 and error bars indicate SEM. **(C)** Cell size of diploid wild type, *rie1Δ*, *cln3Δ*, and *rie1Δ cln3Δ* strains was determined by differential interference contrast microscopy measurements after overnight growth in BYTA (pre-meiotic) medium. The mean is indicated by a black bar and statistical significance (*P < 0.05) was determined by two-sided student's *t* test.

this, we performed polysome profiling in meiosis and mitosis in wild type and *rie1Δ* strains to assess if there were major differences in bulk translational profiles. We observed a pronounced buildup of 80S monosome peaks in *rie1Δ* compared to wild type cells throughout meiosis (Fig. S4 A). On the other hand, the polysome profiles of wild type and *rie1Δ* cells are similar in vegetative cells undergoing mitosis (Fig. S4 B). While our data support the idea that Rie1 is important for translation specifically during gametogenesis, we appreciate that some or all the *rie1Δ* 80S buildup could be explained by pleiotropic defects.

To further investigate the possibility that Rie1 acts as a translational activator, we wanted to test whether Rie1 physically interacts with the translational machinery. We examined the distribution of epitope-tagged Rie1 (Rie1-V5) in cell lysates fractionated on sucrose density gradients, relative to the positions of bulk protein, small ribonuclear particles, ribosomes, and polysomes. We analyzed samples with and without a mild formaldehyde crosslinking treatment which can help detect transient interactions between ribosomes and other factors (Valášek et al., 2007; Wagner et al., 2020). We observed increased abundance of Rie1 in actively translating fractions (i.e., ribosomes and polysomes) in the crosslinked samples throughout pre-meiotic S-phase (Fig. 4, A–C). As some RBPs have the capacity to self-assemble into structures that fractionate as large/dense particles (Berchowitz et al., 2015), we wanted to test whether the sedimentation profile of Rie1 requires intact ribosomes. We assessed the sedimentation of Rie1 in the presence of EDTA, a magnesium chelator that disrupts ribosome structure (Gesteland, 1966). We found that EDTA treatment caused a dramatic change in Rie1 sedimentation to light fractions containing disrupted ribosomal subunits (Fig. S4 C). Together, these results support the idea that the sedimentation profile of Rie1 is likely due to its association with either ribosomes or translating mRNA and not due to hetero- or homotypic assembly of the protein. We next asked whether Ime1 protein expression is affected by the presence or absence of Rie1 outside of the meiotic context. To test this, we placed *IME1* under the control of an inducible *pGAL1-10* promoter in haploid wild type and *rie1Δ* strains harboring the *GAL4.ER* fusion. After induction of *IME1* transcription, we observed that *rie1Δ* cells accumulated less Ime1 protein compared with wild type cells at early timepoints in glucose-containing medium (Fig. 4 D). This result suggests that the effect of Rie1 is independent of the endogenous *IME1* promoter and independent of any upstream signaling cues that drive *IME1* expression (i.e., diploidy or starvation).

To test whether the meiotic transcription of *IME1* target genes is dysregulated in *rie1Δ*, we performed an early meiotic RNA sequencing (RNA-seq) time course in wild type and *rie1Δ*. We confirmed that the presence or absence of Rie1 did not significantly influence abundance of *IME1* mRNA from 0 to 4 h in SPO medium (*IME1* mRNA decreased 0.368-fold in *rie1Δ*; P value 0.67). Using the *UME6* regulon as a reference (Williams et al., 2002), we observed that after 4 h in meiosis, Ime1-Ume6 target transcripts, as a group, were significantly enriched in wild type compared with *rie1Δ* (Fig. S4 D). These results are consistent with the notion that Rie1 acts a posttranscriptional activator of *IME1* and indirectly drives transcription of Ime1/Ume6 targets.

While many proteins in multicellular eukaryotes have a similar domain structure as Rie1, true orthologs are difficult to determine due to their high degree of disorder and commonality of the RRM domain. However, the mammalian proteins most similar to Rie1 are the Bruno-like family of RRM-containing proteins (such as CELF1) which are involved in several RNA-related processes such as translational control and poly(A) tail regulation (Barreau et al., 2006). We hypothesized that Rie1 could influence the length of the *IME1* poly(A) tail, which could, in turn, affect translation efficiency. We tested this hypothesis by performing an oligo(dT)/RNase H Northern blot assay in which meiotic mRNA extracted from wild type and *rie1Δ* was incubated with oligo(dT) DNA and then treated with RNase H which cleaves DNA/RNA hybrids. Because oligo(dT) binds poly(A), RNase H cleaves the poly(A) tail resulting in a Northern blot band shift. This allows estimation of poly(A) tail length of any mRNA based on the band size differences between the oligo(dT)-treated and non-oligo(dT)-treated samples. We found that presence or absence of Rie1 did not affect poly(A) tail length of *IME1* (Fig. S5 A). We conclude that the control of *IME1* by Rie1 does not occur by regulation of poly(A) tail length.

Rie1 forms a complex with the RNA-binding protein Sgn1 to enhance *IME1* translation

To determine co-factors important for Rie1 function, we immunopurified (IPed) Rie1 from cells in the early stages of meiosis (0, 2 h in SPO) and analyzed bound proteins by quantitative mass spectrometry. The most highly enriched protein was another RNA-binding protein Sgn1 which harbors significant similarity to the translation initiation factor eIF4B (Fig. 5 A). Sgn1 is a ~29 kD protein with a single RRM and has been previously identified as a factor that associates with eIF proteins to stimulate translation (Fig. 5 B; Winstall et al., 2000). Notably, our meiotic entry screen identified *sgn1Δ* mutants as having a moderate entry defect (Fig. 1 B). We validated the interaction between Rie1 and Sgn1 by reciprocal co-IP in which FLAG-tagged Sgn1 was pulled down and co-purified V5-tagged Rie1 abundance was measured by immunoblot (Fig. 5 C). We found that essentially all the Rie1 in the lysate was pulled down with Sgn1, implying that the majority of Rie1 present in the cell interacts with Sgn1 (Fig. 5 C). We found that Sgn1 is expressed in both mitotic and meiotic cells with similar abundance in all conditions tested (Fig. 5 D).

If Rie1 and Sgn1 act primarily as a complex, deletion of *SGN1* should not enhance *rie1Δ* meiotic entry defects and vice versa. To test this idea, we assessed *IME1* mRNA/protein accumulation and meiotic progression in wild type, *rie1Δ*, *sgn1Δ*, and *rie1Δ sgn1Δ* strains. We found that both *rie1Δ* and *sgn1Δ* exhibited decreased Ime1 protein levels without corresponding downregulation of *IME1* mRNA levels (Fig. 5, E and F). As indicated by our screen, *sgn1Δ* strains have a less severe phenotype, as measured by Ime1 accumulation and meiotic progression, compared with *rie1Δ* strains (Fig. S5 B). Importantly, the *rie1Δ sgn1Δ* double mutant showed similar defects as *rie1Δ*. These data indicate that Rie1 and Sgn1 both contribute to proper Ime1 expression and meiotic progression but not additively. We also found that Clb3 expression is delayed compared with wild type strains in *rie1Δ* and

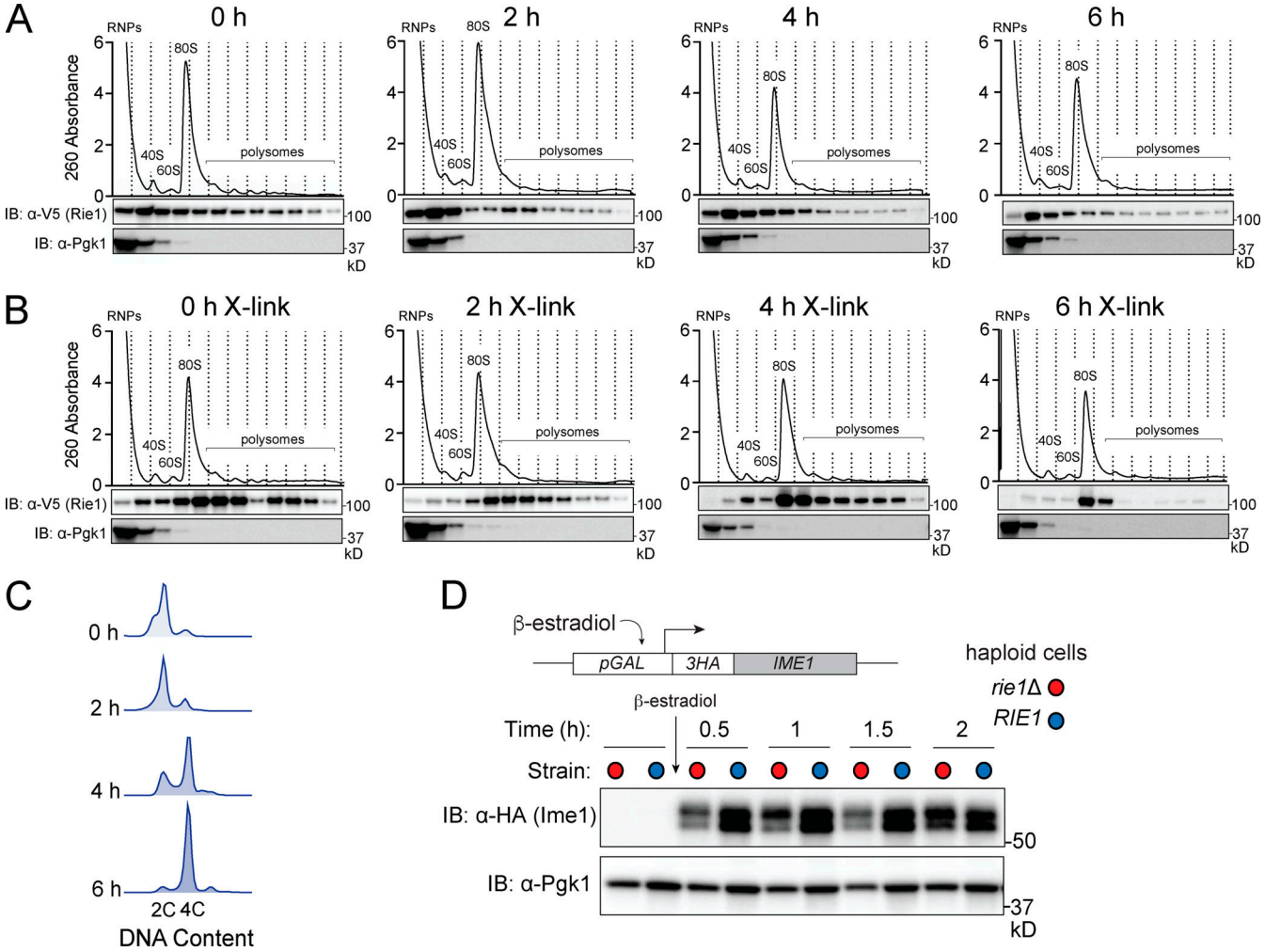

Figure 4. **Rie1 is associated with the translational machinery and positively regulates *IME1*. (A–C)** Strains harboring *RIE1-3V5* (B3114) were induced to sporulate at 30°C and samples were taken either without (A) or with (B) light crosslinking (1% formaldehyde, 15 min on ice). Lysates were fractionated on 10–50% sucrose density gradients with continuous monitoring at 260 nm. Rie1 and Pgk1 (monomeric control) protein levels were determined in each fraction by immunoblot. Positions of the 40S, 60S, 80S, and polysomal ribosome peaks are indicated. **(C)** Progression through pre-meiotic S-phase was determined by flow cytometry. Biological replicates = 3. **(D)** Haploid strains harboring *pGAL-3HA-IME1*, *GAL4.ER*, and either wild type *RIE1* (B2722, blue) or *rie1*Δ (B2719, red) were diluted to 0.5 OD_{600} in SDC. *IME1* was induced by the addition of β-estradiol at 0.5 h. Ime1 and Pgk1 (loading) protein levels were determined at the indicated times. Biological replicates = 3. Source data are available for this figure: SourceData F4.

*sgn1*Δ cells (Fig. S5, C and D). Because Sgn1 contains an RRM, we tested whether it has the capacity to bind *IME1* mRNA. We conducted an EMSA using in vitro transcribed *IME1* mRNA and recombinant Sgn1 purified from *E. coli* (Fig. S5 E). We found that Sgn1 binds *IME1* mRNA compared with the BSA control (Fig. S5 F).

To further understand the physical interaction between Sgn1 and Rie1, we used AlphaFold2 Multimer (Jumper et al., 2021; Evans et al., 2022 *Preprint*; Varadi et al., 2022) to predict the structure of the complex and ChimeraX to visualize the proteins individually and as a complex (Goddard et al., 2018; Pettersen et al., 2021; Fig. 5 G). AlphaFold2 predicts that Sgn1 and Rie1 form a complex (we specified 1:1 stoichiometry based on speculative support from our mass spectrometry data) where the interacting residues primarily exist in unstructured regions of both proteins. The predicted Rie1–Sgn1 structure exhibited clustering of the Rie1 RRM domains at the center of the protein and supports a model where the Sgn1 RRM acts as a clasp around the Rie1 RRM core RNA-binding domains. To test the Rie1–Sgn1 interaction model, we identified and mutated three key residues at the predicted interface between the two proteins (alanine substitutions at Rie1 D429, S433, S435, Fig. 5 G). We then performed co-IP in which V5-tagged Rie1 was pulled down (wild type and mutant) and co-purified FLAG-tagged Sgn1 abundance was measured by immunoblot (Fig. 5 H). In support of our model, we found that *rie1* predicted interface mutations partially disrupted the physical interaction between Rie1 and Sgn1. The effect of the *rie1* interface mutations was particularly evident in the unbound sample, where Sgn1 protein was now detectable in the mutant pulldown. We then tested whether disruption of the Rie1–Sgn1 interface affected Ime1 expression and meiotic progression. We found that *rie1* D429A-S433A-S435A mutants exhibited defective Ime1 accumulation and delayed appearance of bi- and tetranucleate cells compared with wild type (Fig. 5, H

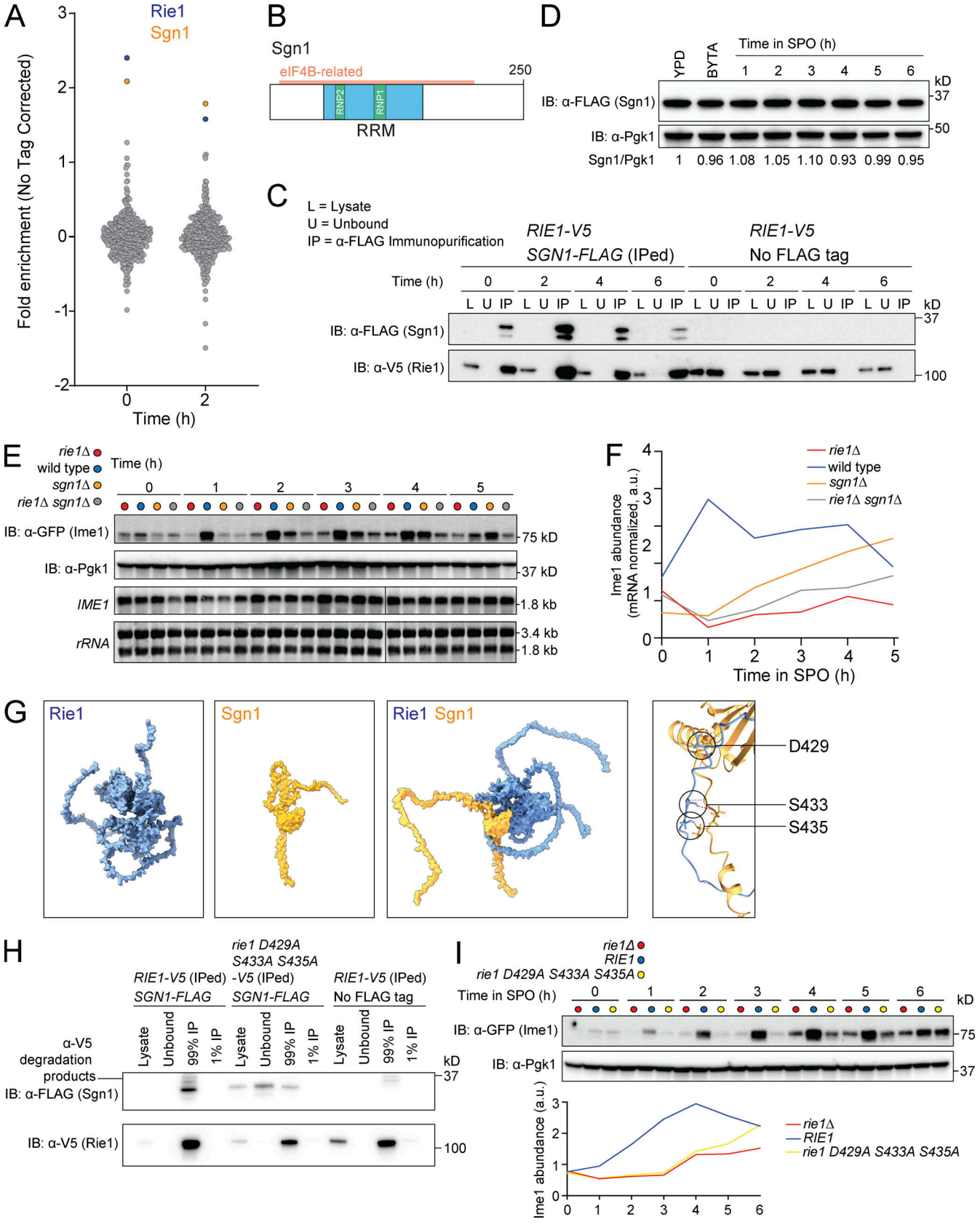

Figure 5. **Rie1 forms a functional complex with the RBP Sgn1. (A)** Strains harboring *RIE1-3V5* (B3114) or wild type *RIE1* (no tag, B47) were induced to sporulate at 30°C and cells were collected at the indicated times. Lysates were prepared and Rie1 IP was conducted under non-denaturing conditions using anti-V5 agarose beads. Precipitated proteins were tandem mass tag(TMT)–labeled and analyzed by mass spectrometry. Shown are the Log_2 ratios of

enrichment over no-tag control for each identified protein (minimum 2 unique peptides). **(B)** Diagram of Sgn1. RRM domain is shown in blue, RNP motifs in green, and eIF4B-related region is outlined in orange. **(C)** Strains harboring *RIE1-3V5* and either *SGN1-FLAG* (B2668) or wild type *SGN1* (B3114) were induced to sporulate at 30°C. Sgn1-FLAG was IPed from meiotic lysate using anti-FLAG agarose beads at the indicated time points. Shown are Sgn1 and Rie1 protein levels by immunoblot (IB) in lysate, unbound, and IP samples. Biological replicates = 2. **(D)** Strains harboring *SGN1-FLAG* (B2668) were grown in either YPD (log phase), BYTA (stationary phase), or induced to sporulate at 30°C. Samples were collected at the indicated times and Sgn1 and Pgk1 (loading) protein levels were determined by immunoblot. Quantifications of Sgn1/Pgk1 compared to YPD (set at 1) are indicated below. **(E and F)** Strains harboring N-terminally tagged *sfGFP-IME1* and *rie1Δ* (B2430, red), wild type *RIE1* and *SGN1* (B2459, blue), *sgn1Δ* (B3375, orange), or *rie1Δ sgn1Δ* (B3378, gray) were induced to sporulate at 30°C. Protein levels of Ime1 and Pgk1 (loading) protein levels were determined by immunoblot and mRNA levels of *IME1* and *rRNA* (loading) were determined by Northern blot. **(F)** Quantification of Ime1 protein levels corrected for *IME1* mRNA levels are shown. Biological replicates = 3. **(G)** AlphaFold2 output of individual Rie1–Sgn1 structures and AlphaFold2 Multimer output of predicted Rie1–Sgn1 complex. Rie1 is shown in blue and Sgn1 is shown in orange. A ribbon diagram zoomed in on the predicted Rie1–Sgn1 interface is shown on right with key interacting residues on Rie1 highlighted. **(H and I)** Strains harboring *SGN1-FLAG* and 3V5 tagged *RIE1* (B2668) or *rie1 D429A*, *S433A*, and *S435A* (B3551) were induced to sporulate at 30°C. *RIE1-3V5* with untagged wild type *SGN1* (no tag control, B3114) was also included. Rie1-3V5 was IPed from meiotic lysate using anti-V5 agarose at the indicated time points. **(H)** Shown are Sgn1 and Rie1 protein levels by immunoblot in lysate, unbound, and 1% IP and 99% IP samples. **(I)** Protein levels of Ime1 and Pgk1 (loading) were determined by immunoblot with quantifications shown below. Source data are available for this figure: SourceData F5.

and I; and Fig. S5 G). Finally, to determine whether Sgn1 influences meiotic entry by affecting cell size, we performed a cell volume analysis of diploid *rie1Δ*, *sgn1Δ*, and *rie1Δ sgn1Δ* cells grown to saturation in acetate-containing medium. We found that none of the mutants have cell volumes that statistically differ from wild type strains under these conditions (Fig. S5 H). Taken together, our results support a model in which Rie1 and Sgn1 form a complex that acts to enforce the meiotic cell fate decision.

Discussion

In this study, we show that two physically interacting RBPs, Rie1 and Sgn1, positively enforce the cell fate decision to enter meiosis in budding yeast. We found that Rie1 and, to a lesser extent, Sgn1 posttranscriptionally enhance expression of Ime1, which encodes the master regulatory transcription factor governing entry into meiosis. Our results support the idea that after pro-meiotic signaling cues, Rie1 and Sgn1 posttranscriptionally enhance Ime1 accumulation, thus contributing to timely meiotic entry. We also determined that the role of Rie1 and Sgn1 in promoting meiotic entry is not a result of a role in *CLN3* repression. We appreciate that Rie1–Sgn1 may have other functions aside from Ime1 activation. *rie1Δ* mutants show slower progression through the meiotic divisions, and Rie1 depletion in meiotic prophase caused later meiosis progression defects. This supports the notion that Rie1 and Sgn1 have additional targets and roles because Rie1 depletion occurred after the function of Ime1 had already been executed.

There are several mechanisms by which the Rie1–Sgn1 complex could promote Ime1 expression. We can rule out that the Rie1–Sgn1 complex acts primarily by restricting *IME1* mRNA decay based on our steady-state Northern blot and RNA-seq mRNA measurements. One possibility would be that Rie1 and Sgn1 affect splicing of *IME1* mRNA, but because *IME1* contains no introns, this can be ruled out. Alternatively, poly(A) tail length of *IME1* could be affected by Rie1 and Sgn1. However, this is not supported by our poly(A) tail assays. Because C-terminally tagged *IME1-3HA* and *pGAL-IME1-3HA* (the *pGAL1-10* promoter swap replaces the *IME1* 5′UTR) are both repressed in *rie1Δ*, we conclude that there is no essential Rie1-responsive element in the *IME1* 5′ or 3′UTRs, which also likely rules out alternative 3′ cleavage. However, it is possible that the HA construct and/or or the *pGAL* 5′UTR contains a Rie1 binding site. We suspect that Rie1–Sgn1 either binds to the coding sequence of the *IME1* mRNA or a generic mRNA feature such as the poly(A) tail. A speculative possibility is that some feature of *IME1* mRNA could make it more susceptible to regulation by Rie1–Sgn1. We have not determined whether Rie1–Sgn1 influences the *IME1* transcription start site. Our preferred hypothesis, supported by the robust polysome association of Rie1, is that Rie1–Sgn1 recruits *IME1* mRNA to ribosomes.

Our results imply that yeast has evolved a way to control meiotic entry via RBPs that are expressed in both mitosis and meiosis. Aside from its role in promoting Ime1 expression, Rie1 functions in vegetative cells. For example, Rie1 colocalizes with stress granules (Buchan et al., 2008; Yahya et al., 2021) and endoplasmic reticulum encountering structures (ERMES; Kojima et al., 2016). Notably, Rie1 overexpression can rescue respiratory growth in ERMES-deficient *mmm1Δ* mutants. While we did not observe any vegetative growth defects in *rie1Δ* cells under the conditions we tested, it is likely that Rie1 has RNA targets which may allow the protein to have distinct roles in both mitosis and meiosis. It is also possible that its role in ERMES function affects meiotic entry. However, this is somewhat complicated by the fact that diploid *rie1Δ* cells grow readily in respiration-requiring media such as YPG, indicating that, overall, mitochondrial function is maintained in *rie1Δ* cells.

Initiation of meiotic entry in a haploid cell is lethal, and it is critical that a cell restricts Ime1 protein expression to meiosis. Several mechanisms, including RNA decay, play important roles in preventing spurious meiotic entry. Many early meiotic mRNAs, including *IME1*, have short half-lives (~3.1 min for *IME1* when expressed in vegetative cells; Surosky and Esposito, 1992). Because both Rie1 and Sgn1 are low-abundance proteins (Rie1 ~500 and Sgn1 ~2,000 molecules/cell as measured by quantitative mass spectrometry in vegetative growth; Kulak et al., 2014), there is strong competition in the cell for Rie1–Sgn1 mRNA binding sites in vegetative cells (~15,000–40,000 mRNA per cell; Holstege et al., 1998; Zenklusen et al., 2008). We observed that Rie1 is upregulated in starvation while Sgn1 abundance is consistent (in conditions tested). Because Rie1 levels are lower than Sgn1 in vegetative growth (Kulak et al., 2014), Rie1 abundance is likely the limiting factor in Rie1–Sgn1 complex

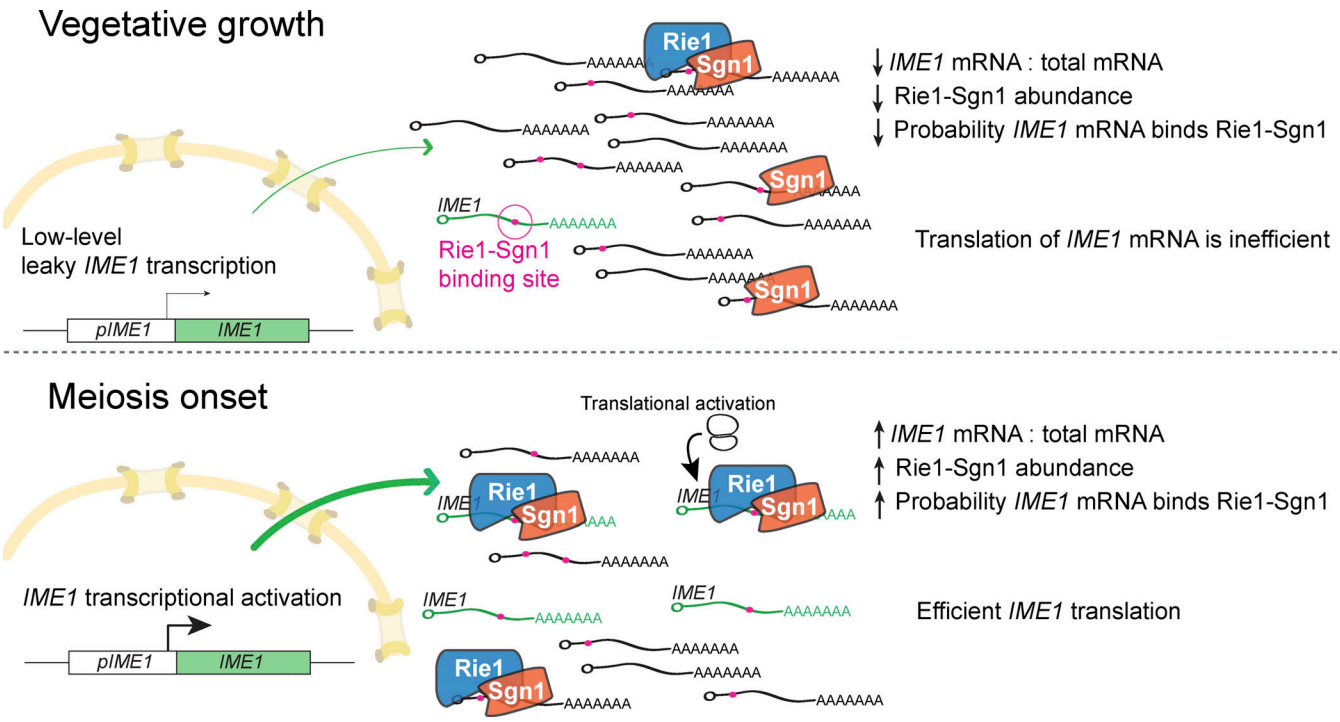

Figure 6. **Model for *IME1* activation by Rie1–Sgn1.** Top: In vegetatively growing cells, *IME1* transcription is repressed and Rie1–Sgn1 abundance is low. *IME1* mRNAs that arise by leaky transcription will have a low probability of encountering Rie1–Sgn1 activators. Bottom: At meiosis onset, *IME1* transcription and Rie1–Sgn1 abundance are increased by pro-sporulation cues. *IME1* transcripts now have a higher probability of encountering Rie1–Sgn1 complexes due to the increased ratio of *IME1* mRNA to total mRNA as well as the increased availability of Rie1–Sgn1.

abundance. We propose that when *IME1* transcription bursts in conjunction with Rie1 upregulation, downstream of nutrient and diploidy cues, the probability that an *IME1* mRNA encounters a Rie1–Sgn1 complex will increase as a function of both *IME1* mRNA and Rie1–Sgn1 complex abundance (Fig. 6). Our model is conceptually similar to the "hungry spliceosome" model proposed by Talkish et al. (2019), which rationalizes why splicing of meiotic genes containing suboptimal introns is more efficient in starvation (Juneau et al., 2007). In this model, spliceosomes are a limiting resource predominantly recruited to optimal splicing sites on abundant transcripts that generally encode ribosomal proteins. During starvation and meiotic entry, transcription of ribosomal protein genes is downregulated, which frees spliceosomes to bind to and splice mRNAs that contain non-consensus splice sites such as *HOP2*, *REC107*, *REC114*, and *DMC1*. Like *IME1*, misexpression of these meiotic factors could be detrimental and the cell has evolved several fail-safe mechanisms, including the Rie1–Sgn1 complex and meiotic introns, to prevent mistimed translation of these transcripts. However, it is equally important that Ime1 expression is robust during the onset of meiosis such that this key developmental decision can be enforced when dictated by environmental conditions. We propose that upregulation of the Rie1–Sgn1 complex during starvation allows sufficient Ime1 protein to trigger Ume6 degradation. This activity triggers *IME2* expression, which results in negative feedback on *IME1* (Rubenstein and Schmidt, 2007) and proper commitment to the meiotic cell fate.

Materials and methods

Yeast strain construction

All strains used in this work were derived from the *S. cerevisiae* SK1 background. We used standard transformation methods (Gietz et al., 1995). Transformations were done in a B1 wild type strain and confirmed by sequencing. Positive transformants were backcrossed with B2 before mating with strains containing desired constructs until the desired genotype was achieved. For point mutants of Rie1, we co-transformed B1 with a plasmid expressing Cas9 and a gRNA sequence targeting the *RIE1* locus and a DNA repair template harboring the desired mutations in *RIE1*. The plasmid also harbored a *kanMX* cassette, allowing for isolation of positive colonies. All strains were confirmed by sequencing.

Yeast media details and culture conditions

All yeast strains were grown at 30°C. For meiotic cultures, strains were inoculated in YEPD (1% yeast extract, 2% peptone, and 2% dextrose) and grown overnight with shaking at 30°C. The following day, the cells were diluted in BYTA (1% yeast extract, 2% tryptone, 1% potassium acetate, 50 mM potassium phthalate) to an OD_{600} of 0.3 and grown overnight with shaking (~16 h). The following morning, cells were washed once with water and resuspended in SPO medium (0.3% potassium acetate, pH 7.0, 0.02% raffinose) at OD_{600} = 1.8 and grown with shaking. Auxin-AID strains were induced to degrade AID-tagged proteins by addition of 0.25 mM Auxin at 5 h. pGAL-NDT80, GAL4.ER

strains were released from G2 arrest by the addition of 1 µM β-estradiol at 6 h.

Meiotic progression analysis and fluorescence microscopy

Cells were fixed in 3.7% formaldehyde. For the analysis of nuclear divisions, Rie1-ENVY, and sfGFP-Ime1, fluorescence microscopy was performed as in Carpenter et al. (2018) with minor modifications. Samples were permeabilized with 1% Triton-X and mounted in 0.1 M KPO_4 (pH 7.5), 1.2 M sorbitol with DAPI. Images were acquired using SoftWoRx (Cytiva) at 100× magnification (Olympus UPLXAPO, numerical aperture 1.45) using a DeltaVision microscope (GE Healthcare) equipped with an EDGE sCMOS 5.5 camera at room temperature (~25°C) and analyzed using FIJI (ImageJ) software. Cells containing one distinct nucleus were classified as uninucleate, cells containing two separate and distinct nuclei were classified as binucleate, and cells containing any more than two separate and distinct nuclei were classified as multinucleate. For live imaging, after 2.5 h of growth in SPO at 30°C, the cells were loaded onto a microfluidics chip (Cell Asic), stage positions were established, and cells were imaged every 7 min for 12 h starting at 3.5 h. Exposure conditions were as follows: FITC 5%T, 0.08 s; mCherry 50%T 0.10 s; 5 z-stacks at 0.2 µm spacing. A max intensity projection was used for analysis.

Fluorescence microscopy signal intensity analysis

GFP signal intensity in the nucleus was quantified using FIJI software. DAPI channel signal was traced in FIJI for each individual cell analyzed (100 cells per condition) and signal intensity in GFP channel was quantified within the border of the DAPI trace to generate numerical values for GFP intensity. The background GFP signal for each image was normalized to the average background signal for each condition.

Denaturing protein sample preparation for immunoblot and immunoprecipitation

Samples were prepared by resuspending the pellet of 4 ml SPO culture in 5% TCA, incubating overnight at 4°C, washing with acetone, and breaking cells using 50 µl acid-washed glass beads (Sigma-Aldrich), 100 µl lysis buffer (10 mM Tris-HCl, 1 mM EDTA, pH 8, 2.75 mM DTT), Halt protease inhibitors (Thermo Fisher Scientific), and a 45-s process in a FastPrep-24 (MP Biomedicals) at maximum speed. We added 50 µl loading buffer (9% SDS, 0.75 mM Bromophenol blue, 187.5 mM Tris-HCl, pH 6.8, 30% glycerol, and 810 mM b-mercaptoethanol); samples were heated at 100°C for 5 min and centrifuged 5 min at 20,000 *g*.

Polynucleotide kinase RNA labeling assay

5 ml of SPO culture (2 h) were UV crosslinked with 750,000 mJ/cm^2, collected by centrifugation, resuspended in 5% TCA, washed once with acetone, and air-dried. A no-UV-crosslinking control was included for each strain analyzed. IP from denatured protein extracts was conducted with modifications. After clarification, extracts were treated with 8 ng/ml RNase A and 4 U Turbo DNase for 15 min at 37°C with shaking at 1,100 rpm. After IP with α-V5 agarose gel (mouse monoclonal, Cat# A7345; Sigma-Aldrich), the gel was washed twice with high salt buffer, twice with low salt buffer, and twice with PNK buffer (50 mM Tris HCl, pH 7.5, 50 mM NaCl, 10 mM $MgCl_2$, 0.5% NP-40) containing 5 mM DTT. Beads were resuspended in PNK buffer + 5 mM DTT, 0.1 mCi/ml [γ-^{32}P]ATP (Perkin Elmer), 1 U/ml T4 PNK (New England Biolabs), and labeled for 15 min at 37°C. Beads were washed with 1 ml PNK buffer to remove unincorporated [γ-^{32}P] ATP and boiled 5 min in 1× SDS-PAGE loading buffer. Samples were then separated by SDS-PAGE and blotted to nitrocellulose. Bound RNA was assessed by phosphorimage, and IP efficiency was determined by the immunoblot protocol listed below. α-V5 (mouse monoclonal, RRID:AB_2556564; Thermo Fisher Scientific) at 1:2,000 was used as a primary antibody and TrueBlot ULTRA α-mouse Ig horseradish peroxidase (HRP; Cat# 18-8816-31; Rockland) used at 1:20,000 for the secondary antibody.

Non-denaturing immunoprecipitation

2 ml of SPO culture was harvested, centrifuged, and flash-frozen in liquid nitrogen. Samples were fully thawed and resuspended in 200 µl NP-40 lysis buffer (50 mM Tris-HCl, pH 7.5, 150 mM NaCl, 1% NP-40, 10% glycerol) and protease inhibitors (1:1,000 DTT, 1:100 Halt protease inhibitors [Thermo Fisher Scientific], and 1 mM PMSF) with 0.5 mm zirconia/silica beads (BioSpec Products). Cells were lysed using a 45-s process in a FastPrep-24 (MP Biomedicals) at maximum speed. The lysates were clarified twice by centrifugation at maximum speed for 10 min at 4°C. Total protein input samples are taken with 10 µl of the lysate and 5 µl loading buffer (9% SDS, 0.75 mM Bromophenol blue, 187.5 mM Tris-HCl, pH 6.8, 30% glycerol, and 810 mM b-mercaptoethanol) and boiled 5 min. The remaining lysate was diluted to 1.5 ml of NP-40 buffer and incubated with 15 µl α-FLAG M2 affinity gel (mouse monoclonal, Cat# A2220; Sigma-Aldrich) or α-V5 agarose (mouse monoclonal, Cat# A7345; Sigma-Aldrich) with rotation for 1 h at 4°C. To pellet affinity gel, samples were centrifuged at 2,000 rpm for 30 s. Unbound protein samples were collected (10 µl), 5 µl loading buffer was added, and samples were boiled for 5 min. The affinity gel was then washed four times with 1 ml NP-40 buffer. The affinity gel was then incubated in 20 µl lysis buffer (10 mM Tris-HCl, 1 mM EDTA, pH 8, 2.75 mM DTT, Halt protease inhibitors [Thermo Fisher Scientific]) and 10 µl loading buffer, boiled for 5 min, and centrifuged 5 min at maximum speed. Samples were then analyzed by the immunoblot protocol listed below, and TrueBlot ULTRA α-mouse Ig HRP (Cat# 18-8816-31; Rockland) used at 1:5,000 for the secondary antibody.

Immunoblot analysis

Polyacrylamide gels were run on a mini or midi gel system (BioRad) with SDS Running Buffer (190 mM glycine, 25 mM Trizma base, 3.5 mM, 1% SDS) using 4–15% gels. Gels were transferred to a nitrocellulose membrane using a semi-dry transfer apparatus (BioRad). α-GFP (mouse monoclonal, Cat# 11814460001; Sigma-Aldrich) was used at 1:1,000, α-Pgk1 (mouse monoclonal, RRID:AB_2532235; Thermo Fisher Scientific) was used at 1:20,000, α-v5 (mouse monoclonal, RRID:AB_2556564; Thermo Fisher Scientific) was used at 1:2,000, α-FLAG (mouse monoclonal, Cat# F7425; Sigma-Aldrich) was used at 1:2,000,

and α-HA (mouse monoclonal, RRID:AB_2565336; BioLegend) was used at 1:1,000. An α-mouse HRP-conjugated secondary antibody (Cytiva) was used at 1:10,000. The signal was visualized using ECL prime chemiluminescence substrate (Cytiva) and acquisition of chemiluminescence images was conducted using an Amersham Imager 600 (GE Healthcare). At least three exposures were taken for each experiment to ensure that our signal did not saturate and that we were in the linear range of the instrument.

Polysome profiling

Approximately, 5 × 10^8 of yeast cells were lysed using a 45-s process in a FastPrep-24 in polysome lysis buffer (20 mM Tris-HCl, pH 7.5, 10 mM magnesium chloride, 50 mM potassium chloride, 10 µg/ml cycloheximide, 1 mM PMSF, 1× Halt protease, and phosphatase inhibitor cocktail [78442; Thermo Fisher Scientific]). Lysate was cleared by centrifugation at 4°C at 20,000 *g* for 10 min. Lysate was loaded on a 10–50% sucrose gradient in polysome lysis buffer. Gradients were centrifuged for 2 h at 38,000 rpm in a Beckman SW41Ti rotor. Fractions were collected using a BioComp gradient station and a BioComp TRiAX flow cell monitoring continuous absorbance at 260 nm. For Western blot analysis, each fraction received 100% TCA to a final concentration of 5% TCA. We then added 50 µl loading buffer (9% SDS, 0.75 mM Bromophenol blue, 187.5 mM Tris-HCl, pH 6.8, 30% glycerol, and 810 mM b-mercaptoethanol); samples were heated at 100°C for 5 min and centrifuged 5 min at 20,000 *g*.

Northern blot analysis

Samples were harvested as 2 ml of SPO culture, centrifuged, and flash-frozen in liquid nitrogen. Pellets were resuspended in 400 µl TES Buffer (10 mM Tris-HCl, pH 7.5, 10 mM EDTA, and 0.5% SDS), 400 µl acid phenol:chloroform 5:1 (Ambion), and 50 µl 0.5 mm zirconia/silica beads (BioSpec). Cells were lysed by shaking at 1,400 rpm for 30 min at 65°C in a Thermomixer (Eppendorf) followed by centrifugation for 5 min at 13,000 *g*, extraction to 1 ml 100% ethanol and 40 µl sodium acetate (pH 5.5), and precipitation at 20°C overnight.

Samples were centrifuged at 13,000 *g* for 20 min, washed with 1 ml 80% ethanol, centrifuged at 13,000 *g* for 5 min, and dried. RNA pellets were resuspended in 25 µl diethyl pyrocarbonate (DEPC) water at 37°C with shaking at 1,000 rpm for 15 min and concentrations were determined using a NanoDrop (Thermo Fisher Scientific). We added 22 µl denaturing mix (15 µl formamide, 5.5 µl formaldehyde, and 1.5 µl 10× MOPS) to 8 mg total RNA in 8 µl and heated at 55°C for 15 min. 20 µl of sample (~5 µg) was resolved on a denaturing agarose gel (1.9% agarose, 3.7% formaldehyde, 13 MOPS buffer) for 2.5 h at 80 V. The gel was blotted to a Hybond membrane (GE Healthcare) by capillary transfer in SSC (1.5 M NaCl, 0.15 M trisodium citrate dihydrate, pH 7). The membrane was incubated in a hybridization buffer (0.25 M Na-phosphate, pH 7.2, 0.25 M NaCl, 1 mM EDTA, 7% SDS, and 5% dextran sulfate) at 65°C probed with α-^{32}P-labeled DNA probes prepared via Amersham Megaprime DNA labeling kit (GE Healthcare) and Illustra ProbeQuant columns (GE Healthcare), transferred to a phosphor screen, and imaged on a Typhoon imager (GE Healthcare).

Blot quantification

Immunoblot and Northern blot experiments were quantified using FIJI software. Signal intensity was normalized to loading control (Pgk1 for immunoblots and rRNA for Northerns).

RNA–protein EMSA

IME1 in vitro transcription

IME1 mRNA (with 5′ and 3′ UTRs) was transcribed in vitro using the MEGAscript T7 kit (Thermo Fisher Scientific). Briefly, an *IME1* DNA template with a T7 promoter sequence was amplified from SK1 genomic DNA by PCR and gel purified. 1 µg of DNA template was used in the in vitro transcription reaction which was incubated at 37°C for 3 h. The reaction was treated with TURBO DNAse to remove the DNA template (37°C, 15 min). RNA was recovered by phenol/chloroform extraction, isopropanol precipitated, washed with 80% ethanol, and resuspended in DEPC-treated water.

Cloning, expression, and purification of Rie1 and Sgn1

Full-length *RIE1 and SGN1* (from *S. cerevisiae* SK1 genomic DNA) was cloned into the first cassette of a pET-Duet plasmid using inverse PCR. The pET-Duet plasmid was previously modified to encode a C-terminal 3C protease cut site) followed by a His tag. For protein expression, the plasmids carrying C-terminally tagged *RIE1* and *SGN1* were transformed into the low background strain (LOBSTR) *E. coli* expression strain containing a RIL plasmid (Kerafast; Andersen et al., 2013). To obtain purified Rie1 and Sgn1, 1 liter of LOBSTR cells containing the *RIE1 or SGN1* plasmids were grown in LB (with 100 µg/ml of ampicillin and 35 µg/ml of chloramphenicol) to an OD_{600} of 0.7 at 37°C, shifted to 18°C for 30 min, and induced with 200 µM IPTG for 18 h. The cells were collected by centrifugation and resuspended in 400 ml of cold lysis buffer (50 mM Tris/HCl, pH 8.0, 500 mM NaCl, 40 mM imidazole, and 5 mM β-mercaptoethanol). The cells were lysed on ice by sonication (Misonix). Cell debris was removed by centrifugation and the supernatant was incubated with 1 ml of equilibrated Ni-Sepharose 6 Fast Flow resin (GE Life Sciences) and gently mixed in batch for 1 h at 4°C. The Ni-resin was collected by centrifugation and placed in a 10-ml polypropylene column (Thermo Fisher Scientific) and washed with 100 column volumes of wash buffer (10 mM Tris/HCl, pH 8.0, 150 mM NaCl, 40 mM imidazole, and 5 mM β-mercaptoethanol). Rie1 and Sgn1 were eluted with 5 ml of elution buffer (10 mM Tris/HCl, pH 8.0, 150 mM NaCl, 300 mM imidazole, and 5 mM β-mercaptoethanol) and analyzed by SDS-PAGE. The eluate was treated with HRV 3C protease (Sino Biological) for 16 h at 4°C to cleave the His tag. Samples were reincubated on Ni-Sepharose to remove the tag and the 3C (contains a His tag), placed in a 10-ml polypropylene column, and the flowthrough was collected and analyzed by SDS-PAGE.

EMSA

5 pmol of *IME1* mRNA (including UTRs) was incubated with purified protein (gradient from 100, 50, 10, 5, 1, 0.5, 0.1 pmol) in a binding buffer (40 mM Tris HCl, pH 8.0, 30 mM KCl, 1 mM $MgCl_2$, 0.01% NP-40, 1 mM DTT) for 45 min at 30°C. After incubation, samples were diluted with 4 µl loading buffer (60 mM

KCl, 10 mM Tris HCl, pH 7.6, 5% glycerol, 0.01% xylene cyanol, and 0.01% Bromophenol blue). 10 µl of each sample was separated on a 1% agarose Tris-Borate-EDTA gel which was stained with SYBR Gold (Thermo Fisher Scientific) and visualized on a UV imager.

Flow cytometry analysis

Samples were harvested as 1.5 ml of SPO culture, centrifuged for 1 min at 3,000 *g*, resuspended in 1 ml 70% ethanol, and left overnight to fix. Samples were twice centrifuged, aspirated, and resuspended in 800 µl 50 mM sodium citrate (pH 7). Cells were sonicated (S-4000; Misonix) for 10 s at 2 amplitude. 200 µl of RNAse buffer (50 mM sodium citrate, 0.25 mg/ml RNAse A [Millipore]) was added to the sample and incubated at 37°C overnight. Samples were incubated for 1 h at 37°C with 5 µl of proteinase K (Millipore). Samples were pelleted at 3,000 *g*, aspirated, resuspended in SYTOX buffer (500 µl 50 mM sodium citrate, pH 7, 1 µM SYTOX green [Invitrogen]), transferred to 5 ml polystyrene tubes (Falcon), and allowed to stain at room temperature for 1 h protected from light. Before measuring, samples were sonicated for 10 s at 2 amplitude, and SYTOX staining for 30,000 cells was measured on a flow cytometer (Accuri) with gating to remove debris.

Rie1 IP and quantitative mass spectrometry

For native Rie1 IP, 25 ml meiotic culture was pelleted, washed once with Tris (pH 7.5), transferred into a 2 ml tube, and snap-frozen in liquid nitrogen for later processing. Cells were broken with Zirconia/Silica beads in 200 µl NP-40 Lysis Buffer (50 mM Tris, pH 7.5, 150 mM NaCl, 1% NP-40, 10% glycerol) containing 1 mM DTT and Halt protease inhibitors (Thermo Fisher Scientific). After breaking, extracts were cleared twice by centrifugation at maximum speed at 4°C in a benchtop centrifuge. IPs were performed in extract diluted to 1 ml in NP-40 buffer. Rie1-3V5 was IPed at 4°C for 2 h using 20 µl of anti-V5-agarose (Sigma-Aldrich). After incubation, beads were washed four times with NP-40 buffer, twice in Buffer 2 (50 mM Tris, pH 7.5, 150 mM NaCl, 10 mM MgCl2, 0.05% NP-40, and 5% glycerol), and twice in Buffer 3 (50 mM Tris, pH 7.5, 150 mM NaCl, 10 mM MgCl2, and 5% glycerol). After the last wash, the wash buffer was aspirated completely and the beads were resuspended in 80 µl trypsin buffer (2 M urea, 50 mM Tris, pH 7.5, 5 µg/ml trypsin) to digest the bound proteins at 37°C for 1 h with agitation. The beads were centrifuged at 100 rcf for 30 s and the partially digested proteins (the supernatant) were collected. The beads were then washed twice with 60 µl urea buffer (2 M urea, 50 mM Tris, pH 7.5). The supernatant of both washes was collected and combined with the partially digested proteins (final volume 200 µl). After brief centrifugation, the combined partially digested proteins were cleared from residual beads and frozen in liquid nitrogen.

100 µl of the partially digested proteins were thawed and disulfide bonds were reduced with 5 mM DTT and cysteines were subsequently alkylated with 10 mM iodoacetamide. Samples were further digested by adding 0.5 µg sequencing grade modified trypsin (Promega) at 25°C. After 16 h of digestion, samples were acidified with 1% formic acid (final concentration). Tryptic peptides were desalted on C18 StageTips according to Rappsilber et al. (2007) and evaporated to dryness in a vacuum concentrator. The desalted peptides were labeled with the TMT11plex mass tag labeling reagent according to the manufacturer's instructions (Thermo Fisher Scientific) with small modifications. Briefly, peptides were dissolved in 30 µl of 50 mM Hepes (pH 8.5) solution and the TMT-11plex reagent was added in 12.3 µl of MeCN. After 1 h incubation, the reaction was stopped with 2.5 µl 5% hydroxylamine for 15 min at 25°C. Differentially labeled peptides were mixed for each replicate (see mixing scheme below) and subsequently desalted on C18 StageTips (Rappsilber et al., 2007), evaporated to dryness in a vacuum concentrator, and reconstituted in 20 µl 3% acetonitrile and 0.1% formic acid.

Liquid chromatography–tandem mass spectrometry was performed as previously described with minor modifications (Cheng et al., 2018; Keshishian et al., 2015). The samples were analyzed on an Eksigent nano LC-415 HPLC system (Sciex) coupled via a 25 cm C18 column (inner diameter 100 µm packed in-house with 2.4 µm ReproSil-Pur C18-AQ medium; Dr. Maisch GmbH) to a benchtop Orbitrap Q Exactive HF mass spectrometer (Thermo Fisher Scientific). Peptides were separated at a flow rate of 250 nl/min with a linear 106 min gradient from 2% to 25% solvent B (100% acetonitrile, 0.1% formic acid), followed by a linear 5-min gradient from 25% to 85% solvent B. Each sample was run for 140 min, including sample loading and column equilibration times. Data were acquired in a data-dependent mode using Xcalibur 2.8 software. MS1 Spectra were measured with a resolution of 60,000, an automatic gain control target of 3e6, and a mass range from 375 to 2,000 m/z. Up to 15 MS2 spectra per duty cycle were triggered at a resolution of 60,000, an automatic gain control target of 2e5, an isolation window of 1.6 m/z, and a normalized collision energy of 36.

All raw data were analyzed with MaxQuant software version 1.6.0.16 (Cox and Mann, 2008) using a UniProt yeast database (release 2014_09, strain ATCC 204508/S288c), and tandem mass spectrometry searches were performed with the following parameters: TMT-11plex labeling on the MS2 level, oxidation of methionine and protein N-terminal acetylation as variable modifications; carbamidomethylation as fixed modification; Trypsin/P as the digestion enzyme; precursor ion mass tolerances of 20 ppm for the first search (used for nonlinear mass recalibration) and 4.5 ppm for the main search; and a fragment ion mass tolerance of 20 ppm. For identification, we applied a maximum false discovery rate of 1% separately on protein and peptide levels. We required one or more unique/razor peptides for protein identification.

Finally, the TMT MS2 intensities were normalized such that at each condition these intensity values added up to exactly 1,000,000; therefore, each protein group value can be regarded as a normalized microshare (we did this separately for each TMT channel for all proteins that made our filter cutoff in all the TMT channels).

Oligo(dT)/RNase H Northern blot assay

10 µg of purified RNA samples for each condition (wt and *rie1Δ*) was transferred to a PCR tube (VWR). Then 1.7 µl of primer was

added to each tube. 3.3 µl oligo dT or water (+/− oligo dT samples) was then added. Samples were then flick mixed, briefly spun down, and incubated at 65°C for 5 min. Samples were removed from heat and placed on ice before RNAse H digestion with 1.6 µl RNAse H, 1.6 µl RNAse H 10× buffer, and water to 16 µl total volume. The samples were again flick mixed, spun down, and then incubated at 37°C for 30 min. The samples were run as in the above Northern blot protocol, with the only differences being 44 µl of standard denaturation mix was used and the final gel was a 2% agarose gel, which was run for 3 h.

RNA-seq and alignment

Briefly, poly-A pull-down was used to enrich mRNAs from total RNA samples and proceed on library preparation by using Illumina TruSeq RNA prep kit. Libraries were sequenced using paired-end sequencing (100 bp) in multiplex using Illumina NovaSeq at Columbia Genome Center. Real-time analysis (RTA, Illumina) was used for base calling and bcl2fastq2 (version 2.17) for converting BCL to fastq format, coupled with adaptor trimming. Sequencing reads were mapped onto SK1 genome reference (Yue et al., 2017) using STAR (Dobin et al., 2013) with the following parameters: multiple alignments allowed: 20; multiple alignment retained: 1; order of multiple alignments: Random (--outMultimapperOrder Random --outSAMmultNmax 1 --outFilterMultimapNmax 20 --outFilterScoreMinOverLread 0.3 --outFilterMatchNminOverLread 0.1 --seedSearchStartLmax 20 --seedSearchStartLmaxOverLread 0.2 --alignSJoverhangMin 1 --alignSJDBoverhangMin 1) while other parameters were set to defaults. Reads count were scaled by count per millions.

Differential RNA-seq analysis

The tool featureCounts (Liao et al., 2014) was used to determine the number of reads mapped to each transcript using the default parameters except -O allowMultiOverlap. Volcano plots were produced using the output of DESeq2 (Love et al., 2014). To determine whether the overall enrichment of the *UME6* regulon, as a group, in wild type vs. *rie1*Δ is significant, we compared the mean enrichment of the *UME6* regulon (38 genes) to random expectations. Briefly, we sampled enrichment values of 38 randomized genes 10,000 times. From these randomizations, we generated a distribution with a defined mean and standard deviation. We then generated a z-score and corresponding P value from our observed enrichment value for the *UME6* regulon (mean fold enrichment 0.561).

Statistical methods

Statistical significance was determined by Student's *t* test (two-sided), Mann-Whitney test, or Z test statistic as indicated. We used Prism 9 software to determine whether our data met the assumptions of each statistical approach. In cases of non-normal data distributions, we analyzed statistical significance using a non-parametric Mann–Whitney test. The number of biological replicates and exact values of *n* are indicated in figure legends where applicable.

Online supplemental material

The supplementary material for this paper includes five figures. Fig. S1 contains a graphical representation of RBP genes used in our screen, analyses of Rie1 abundance and RNA binding, and Rie1 localization analysis. Fig. S2 provides supporting data for the assertions that Rie1 affects Ime2 and Ime4 levels and binds *IME1* mRNA. Fig. S3 is related to Fig. 2, C–F, and supports the argument that *rie1* mutants accumulate lower levels of Ime1 protein using N-terminal sfGFP-tagged Ime1 driven by its endogenous promoter. Fig. S4 supports the idea that, during meiosis, global translation is decreased in *rie1*Δ, sedimentation of Rie1 into a velocity gradient depends on intact ribosomes, and that levels of *IME1* target mRNAs are down in *rie1*Δ. Fig. S5 is related to Fig. 5 and supports the argument that Rie1 interacts with Sgn1 to promote *IME1* translation and meiotic entry. The supplementary material also includes two videos. These videos are examples of time-lapse epifluorescence microscopy of wild type (Video 1) and *rie1*Δ (Video 2) used for the analyses in Fig. 1. The supplement also contains four tables detailing the strains and data used for our meiotic entry screen (Table S1), the strains used in this study (Table S2), a table of reagents used in this study (Table S3), and RNA-seq raw data (Table S4).

Data availability

The data underlying all figures are available in the published article and its online supplemental material. The RNA-seq data underlying Fig. S4 D are openly available at the NIH BioProject repository (accession: PRJNA902727).

Acknowledgments

We would like to thank Marko Jovanovic for mass spectrometry sample prep and analysis, and Dr. Gerson Rothschild for help with flow cytometry analysis. We would also like to thank Eric Schon, Rodney Rothstein, and members of the Berchowitz lab for valuable discussions and for critical reading of the manuscript.

This research is supported by the Schaefer Research Scholars Program, the Hirschl Family Trust, and the National Institutes of Health grant R35 GM124633 to L.E. Berchowitz.

Author contributions: Conceptualization, A. Gaspary and L.E. Berchowitz; Methodology A. Gaspary and L.E. Berchowitz; Formal analysis, A. Gaspary and R. Laureau; Investigation, A. Gaspary, A. Dyatel, G. Dursuk, Y. Simon, and L.E. Berchowitz; Writing—Original Draft, A. Gaspary; Writing—Review and Editing, A. Gaspary and L.E. Berchowitz; Visualization, A. Gaspary, R. Laureau, and L.E. Berchowitz; Supervision, L.E. Berchowitz; Funding Acquisition, L.E. Berchowitz.

Disclosures: The authors declare no competing interests exist.

Submitted: 17 February 2023
Revised: 28 June 2023
Accepted: 8 August 2023

References

Andersen, K.R., N.C. Leksa, and T.U. Schwartz. 2013. Optimized E. coli expression strain LOBSTR eliminates common contaminants from His-tag purification. *Proteins*. 81(11):1857–1861. https://doi.org/10.1002/prot.24364

Barreau, C., L. Paillard, A. Méreau, and H.B. Osborne. 2006. Mammalian CELF/Bruno-like RNA-binding proteins: Molecular characteristics and biological functions. *Biochimie*. 88:515–525. https://doi.org/10.1016/j.biochi.2005.10.011

Benjamin, K.R., C. Zhang, K.M. Shokat, and I. Herskowitz. 2003. Control of landmark events in meiosis by the CDK Cdc28 and the meiosis-specific kinase Ime2. *Genes Dev*. 17:1524–1539. https://doi.org/10.1101/gad.1101503

Berchowitz, L.E., A.S. Gajadhar, F.J. van Werven, A.A. De Rosa, M.L. Samoylova, G.A. Brar, Y. Xu, C. Xiao, B. Futcher, J.S. Weissman, et al. 2013. A developmentally regulated translational control pathway establishes the meiotic chromosome segregation pattern. *Genes Dev*. 27:2147–2163. https://doi.org/10.1101/gad.224253.113

Berchowitz, L.E., G. Kabachinski, M.R. Walker, T.M. Carlile, W.V. Gilbert, T.U. Schwartz, and A. Amon. 2015. Regulated Formation of an amyloid-like translational repressor governs gametogenesis. *Cell*. 163:406–418. https://doi.org/10.1016/j.cell.2015.08.060

Brar, G.A., M. Yassour, N. Friedman, A. Regev, N.T. Ingolia, and J.S. Weissman. 2012. High-resolution view of the yeast meiotic program revealed by ribosome profiling. *Science*. 335:552–557. https://doi.org/10.1126/science.1215110

Buchan, J.R., D. Muhlrad, and R. Parker. 2008. P bodies promote stress granule assembly in Saccharomyces cerevisiae. *J. Cell Biol*. 183:441–455. https://doi.org/10.1083/jcb.200807043

Cappell, S.D., M. Chung, A. Jaimovich, S.L. Spencer, and T. Meyer. 2016. Irreversible APC(Cdh1) inactivation underlies the point of No return for cell-cycle entry. *Cell*. 166:167–180. https://doi.org/10.1016/j.cell.2016.05.077

Carlile, T.M., and A. Amon. 2008. Meiosis I is established through division-specific translational control of a cyclin. *Cell*. 133:280–291. https://doi.org/10.1016/j.cell.2008.02.032

Carpenter, K., R.B. Bell, J. Yunus, A. Amon, and L.E. Berchowitz. 2018. Phosphorylation-mediated clearance of amyloid-like assemblies in meiosis. *Dev. Cell*. 45:392–405.e6. https://doi.org/10.1016/j.devcel.2018.04.001

Cheng, Q.-Y., J. Xiong, F. Wang, B.-F. Yuan, and Y.-Q. Feng. 2018. Chiral derivatization coupled with liquid chromatography/mass spectrometry for determining ketone metabolites of hydroxybutyrate enantiomers. *Chin. Chem. Lett*. 29:115–118. https://doi.org/10.1016/j.cclet.2017.06.009

Clancy, M.J., M.E. Shambaugh, C.S. Timpte, and J.A. Bokar. 2002. Induction of sporulation in Saccharomyces cerevisiae leads to the formation of N6-methyladenosine in mRNA: A potential mechanism for the activity of the IME4 gene. *Nucleic Acids Res*. 30:4509–4518. https://doi.org/10.1093/nar/gkf573

Cox, J., and M. Mann. 2008. MaxQuant enables high peptide identification rates, individualized p.p.b.-range mass accuracies and proteome-wide protein quantification. *Nat. Biotechnol*. 26:1367–1372. https://doi.org/10.1038/nbt.1511

Dalton, S. 2015. Linking the cell cycle to cell fate decisions. *Trends Cell Biol*. 25:592–600. https://doi.org/10.1016/j.tcb.2015.07.007

Day, A., J. Markwardt, R. Delaguila, J. Zhang, K. Purnapatre, S.M. Honigberg, and B.L. Schneider. 2004. Cell size and Cln-Cdc28 complexes mediate entry into meiosis by modulating cell growth. *Cell Cycle*. 3:1433–1439. https://doi.org/10.4161/cc.3.11.1205

Deng, C., and W.S. Saunders. 2001. RIM4 encodes a meiotic activator required for early events of meiosis in Saccharomyces cerevisiae. *Mol. Genet. Genomics*. 266:497–504. https://doi.org/10.1007/s004380100571

Dobin, A., C.A. Davis, F. Schlesinger, J. Drenkow, C. Zaleski, S. Jha, P. Batut, M. Chaisson, and T.R. Gingeras. 2013. STAR: Ultrafast universal RNA-seq aligner. *Bioinformatics*. 29:15–21. https://doi.org/10.1093/bioinformatics/bts635

Dreyfuss, G., V.N. Kim, and N. Kataoka. 2002. Messenger-RNA-binding proteins and the messages they carry. *Nat. Rev. Mol. Cell Biol*. 3:195–205. https://doi.org/10.1038/nrm760

Ephrussi, B., and H. Hottinguer. 1951. On an unstable cell state in yeast. *Cold Spring Harb. Symp. Quant. Biol*. 16:75–85. https://doi.org/10.1101/SQB.1951.016.01.007

Evans, R., M. O'Neill, A. Pritzel, N. Antropova, A. Senior, T. Green, A. Žídek, R. Bates, S. Blackwell, J. Yim, et al. 2022. Protein complex prediction with AlphaFold-Multimer. *bioRxiv*. (Preprint posted March 10, 2022). https://doi.org/10.1101/2021.10.04.463034

Finn, R.D., A. Bateman, J. Clements, P. Coggill, R.Y. Eberhardt, S.R. Eddy, A. Heger, K. Hetherington, L. Holm, J. Mistry, et al. 2014. Pfam: The protein families database. *Nucleic Acids Res*. 42:D222–D230. https://doi.org/10.1093/nar/gkt1223

Furlong, E.E. 2010. The importance of being specified: Cell fate decisions and their role in cell biology. *Mol. Biol. Cell*. 21:3797–3798. https://doi.org/10.1091/mbc.e10-05-0436

Garí, E., T. Volpe, H. Wang, C. Gallego, B. Futcher, and M. Aldea. 2001. Whi3 binds the mRNA of the G1 cyclin CLN3 to modulate cell fate in budding yeast. *Genes Dev*. 15:2803–2808. https://doi.org/10.1101/gad.203501

Gelbart, M.E., T. Rechsteiner, T.J. Richmond, and T. Tsukiyama. 2001. Interactions of Isw2 chromatin remodeling complex with nucleosomal arrays: analyses using recombinant yeast histones and immobilized templates. *Mol. Cell. Biol*. 21(6):2098–2106. https://doi.org/10.1128/MCB.21.6.2098-2106.2001

Gesteland, R.F. 1966. Unfolding of Escherichia coli ribosomes by removal of magnesium. *J. Mol. Biol*. 18:356–371. https://doi.org/10.1016/S0022-2836(66)80253-X

Gietz, R.D., R.H. Schiestl, A.R. Willems, and R.A. Woods. 1995. Studies on the transformation of intact yeast cells by the LiAc/SS-DNA/PEG procedure. *Yeast*. 11:355–360. https://doi.org/10.1002/yea.320110408

Glisovic, T., J.L. Bachorik, J. Yong, and G. Dreyfuss. 2008. RNA-binding proteins and post-transcriptional gene regulation. *FEBS Lett*. 582:1977–1986. https://doi.org/10.1016/j.febslet.2008.03.004

Goddard, T.D., C.C. Huang, E.C. Meng, E.F. Pettersen, G.S. Couch, J.H. Morris, and T.E. Ferrin. 2018. UCSF ChimeraX: Meeting modern challenges in visualization and analysis. *Protein Sci. Publ. Protein Soc*. 27:14–25. https://doi.org/10.1002/pro.3235

Groth, P., S. Ausländer, M.M. Majumder, N. Schultz, F. Johansson, E. Petermann, and T. Helleday. 2010. Methylated DNA causes a physical block to replication forks independently of damage signalling, O(6)-methylguanine or DNA single-strand breaks and results in DNA damage. *J. Mol. Biol*. 402:70–82. https://doi.org/10.1016/j.jmb.2010.07.010

Guo, G., M. Huss, G.Q. Tong, C. Wang, L. Li Sun, N.D. Clarke, and P. Robson. 2010. Resolution of cell fate decisions revealed by single-cell gene expression analysis from zygote to blastocyst. *Dev. Cell*. 18:675–685. https://doi.org/10.1016/j.devcel.2010.02.012

Guttmann-Raviv, N., S. Martin, and Y. Kassir. 2002. Ime2, a meiosis-specific kinase in yeast, is required for destabilization of its transcriptional activator, Ime1. *Mol. Cell. Biol*. 22:2047–2056. https://doi.org/10.1128/MCB.22.7.2047-2056.2002

Hartwell, L.H. 1974. Saccharomyces cerevisiae cell cycle. *Bacteriol. Rev*. 38:164–198. https://doi.org/10.1128/br.38.2.164-198.1974

Herskowitz, I.. 1988. Life cycle of the budding yeast Saccharomyces cerevisiae. *Microbiol. Rev*. 52:536–553. https://doi.org/10.1128/mr.52.4.536-553.1988

Hetz, C. 2012. The unfolded protein response: Controlling cell fate decisions under ER stress and beyond. *Nat. Rev. Mol. Cell Biol*. 13:89–102. https://doi.org/10.1038/nrm3270

Holstege, F.C.P., E.G. Jennings, J.J. Wyrick, T.I. Lee, C.J. Hengartner, M.R. Green, T.R. Golub, E.S. Lander, and R.A. Young. 1998. Dissecting the regulatory circuitry of a eukaryotic genome. *Cell*. 95:717–728. https://doi.org/10.1016/S0092-8674(00)81641-4

Hongay, C.F., P.L. Grisafi, T. Galitski, and G.R. Fink. 2006. Antisense transcription controls cell fate in Saccharomyces cerevisiae. *Cell*. 127:735–745. https://doi.org/10.1016/j.cell.2006.09.038

Honigberg, S.M., and K. Purnapatre. 2003. Signal pathway integration in the switch from the mitotic cell cycle to meiosis in yeast. *J. Cell Sci.*. 116:2137–2147. https://doi.org/10.1242/jcs.00460

Jumper, J., R. Evans, A. Pritzel, T. Green, M. Figurnov, O. Ronneberger, K. Tunyasuvunakool, R. Bates, A. Žídek, A. Potapenko, et al. 2021. Highly accurate protein structure prediction with AlphaFold. *Nature*. 596:583–589. https://doi.org/10.1038/s41586-021-03819-2

Juneau, K., C. Palm, M. Miranda, and R.W. Davis. 2007. High-density yeast-tiling array reveals previously undiscovered introns and extensive regulation of meiotic splicing. *Proc. Natl. Acad. Sci. USA*. 104:1522–1527. https://doi.org/10.1073/pnas.0610354104

Kahana, S., L. Pnueli, P. Kainth, H.E. Sassi, B. Andrews, and Y. Kassir. 2010. Functional dissection of IME1 transcription using quantitative promoter-reporter screening. *Genetics*. 186:829–841. https://doi.org/10.1534/genetics.110.122200

Kane, S.M., and R. Roth. 1974. Carbohydrate metabolism during ascospore development in yeast. *J. Bacteriol*. 118:8–14. https://doi.org/10.1128/jb.118.1.8-14.1974

Kassir, Y., D. Granot, and G. Simchen. 1988. IME1, a positive regulator gene of meiosis in S. cerevisiae. *Cell*. 52:853–862. https://doi.org/10.1016/0092-8674(88)90427-8

Keshishian, H., M.W. Burgess, M.A. Gillette, P. Mertins, K.R. Clauser, D.R. Mani, E.W. Kuhn, L.A. Farrell, R.E. Gerszten, and S.A. Carr. 2015. Multiplexed, quantitative workflow for sensitive biomarker discovery in plasma yields novel candidates for early myocardial injury. *Mol. Cell. Proteomics*. 14:2375–2393. https://doi.org/10.1074/mcp.M114.046813

Kilian, K.A., B. Bugarija, B.T. Lahn, and M. Mrksich. 2010. Geometric cues for directing the differentiation of mesenchymal stem cells. *Proc. Natl. Acad. Sci. USA*. 107:4872–4877. https://doi.org/10.1073/pnas.0903269107

Kim, S.J., and R. Strich. 2016. Rpl22 is required for IME1 mRNA translation and meiotic induction in S. cerevisiae. *Cell Div.* 11:10. https://doi.org/10.1186/s13008-016-0024-3

Kojima, R., S. Kajiura, H. Sesaki, T. Endo, and Y. Tamura. 2016. Identification of multi-copy suppressors for endoplasmic reticulum-mitochondria tethering proteins in Saccharomyces cerevisiae. *FEBS Lett.* 590: 3061–3070. https://doi.org/10.1002/1873-3468.12358

Kulak, N.A., G. Pichler, I. Paron, N. Nagaraj, and M. Mann. 2014. Minimal, encapsulated proteomic-sample processing applied to copy-number estimation in eukaryotic cells. *Nat. Methods*. 11:319–324. https://doi.org/10.1038/nmeth.2834

Liao, Y., G.K. Smyth, and W. Shi. 2014. featureCounts: an efficient general purpose program for assigning sequence reads to genomic features. *Bioinformatics*. 30:923–930. https://doi.org/10.1093/bioinformatics/btt656

Love, M.I., W. Huber, and S. Anders. 2014. Moderated estimation of fold change and dispersion for RNA-seq data with DESeq2. *Genome Biol.* 15: 550. https://doi.org/10.1186/s13059-014-0550-8

Mallory, M.J., K.F. Cooper, and R. Strich. 2007. Meiosis-specific destruction of the Ume6p repressor by the Cdc20-directed APC/C. *Mol. Cell*. 27: 951–961. https://doi.org/10.1016/j.molcel.2007.08.019

Maris, C., C. Dominguez, and F.H. Allain. 2005. The RNA recognition motif, a plastic RNA-binding platform to regulate post-transcriptional gene expression. *FEBS J*. 272(9):2118–2131. https://doi.org/10.1111/j.1742-4658.2005.04653.x

Miller, M.P., E. Ünal, G.A. Brar, and A. Amon. 2012. Meiosis I chromosome segregation is established through regulation of microtubule-kinetochore interactions. *Elife*. 1:e00117. https://doi.org/10.7554/eLife.00117

Mitchell, A.P., and K.S. Bowdish. 1992. Selection for early meiotic mutants in yeast. *Genetics*. 131:65–72. https://doi.org/10.1093/genetics/131.1.65

Mitchell, A.P., S.E. Driscoll, and H.E. Smith. 1990. Positive control of sporulation-specific genes by the IME1 and IME2 products in Saccharomyces cerevisiae. *Mol. Cell. Biol.* 10:2104–2110. https://doi.org/10.1128/mcb.10.5.2104-2110.1990

Morawska, M., and H.D. Ulrich. 2013. An expanded tool kit for the auxin-inducible degron system in budding yeast. *Yeast*. 30(9):341–351. https://doi.org/10.1002/yea.2967

Nachman, I., A. Regev, and S. Ramanathan. 2007. Dissecting timing variability in yeast meiosis. *Cell*. 131:544–556. https://doi.org/10.1016/j.cell.2007.09.044

Nishimura, K., T. Fukagawa, H. Takisawa, T. Kakimoto, and M. Kanemaki. 2009. An auxin-based degron system for the rapid depletion of proteins in nonplant cells. *Nat. Methods*. 6:917–922. https://doi.org/10.1038/nmeth.1401

Pettersen, E.F., T.D. Goddard, C.C. Huang, E.C. Meng, G.S. Couch, T.I. Croll, J.H. Morris, and T.E. Ferrin. 2021. UCSF ChimeraX: Structure visualization for researchers, educators, and developers. *Protein Sci. Publ. Protein Soc.* 30:70–82. https://doi.org/10.1002/pro.3943

Purnapatre, K., S. Piccirillo, B.L. Schneider, and S.M. Honigberg. 2002. The CLN3/SWI6/CLN2 pathway and SNF1 act sequentially to regulate meiotic initiation in Saccharomyces cerevisiae. *Genes Cells*. 7:675–691. https://doi.org/10.1046/j.1365-2443.2002.00551.x

Rappsilber, J., M. Mann, and Y. Ishihama. 2007. Protocol for micro-purification, enrichment, pre-fractionation and storage of peptides for proteomics using StageTips. *Nat. Protoc.* 2:1896–1906. https://doi.org/10.1038/nprot.2007.261

Rubenstein, E.M., and M.C. Schmidt. 2007. Mechanisms regulating the protein kinases of Saccharomyces cerevisiae. *Eukaryot. Cell*. 6:571–583. https://doi.org/10.1128/EC.00026-07

Schindelin, J., I. Arganda-Carreras, E. Frise, V. Kaynig, M. Longair, T. Pietzsch, S. Preibisch, C. Rueden, B. Saalfeld, B. Schmid, et al. 2012. Fiji: an open-source platform for biological-image analysis. *Nat. Methods*. 9(7):676–682. https://doi.org/10.1038/nmeth.2019

Sherman, A., M. Shefer, S. Sagee, and Y. Kassir. 1993. Post-transcriptional regulation of IME1 determines initiation of meiosis in Saccharomyces cerevislae. *Mol. Gen. Genet.* 237:375–384. https://doi.org/10.1007/BF00279441

Slubowski, C.J., A.D. Funk, J.M. Roesner, S.M. Paulissen, and L.S. Huang. 2015. Plasmids for C-terminal tagging in Saccharomyces cerevisiae that contain improved GFP proteins, Envy and Ivy. *Yeast*. 32:379–387. https://doi.org/10.1002/yea.3065

Smith, H.E., S.S. Su, L. Neigeborn, S.E. Driscoll, and A.P. Mitchell. 1990. Role of IME1 expression in regulation of meiosis in Saccharomyces cerevisiae. *Mol. Cell. Biol.* 10:6103–6113. https://doi.org/10.1128/MCB.10.12.6103

Soushko, M., and A.P. Mitchell. 2000. An RNA-binding protein homologue that promotes sporulation-specific gene expression in Saccharomyces cerevisiae. *Yeast*. 16:631–639. https://doi.org/10.1002/(SICI)1097-0061(200005)16:7<631::AID-YEA559>3.0.CO;2-U

Surosky, R.T., and R.E. Esposito. 1992. Early meiotic transcripts are highly unstable in Saccharomyces cerevisiae. *Mol. Cell. Biol.* 12:3948–3958. https://doi.org/10.1128/mcb.12.9.3948-3958.1992

Talkish, J., H. Igel, R.J. Perriman, L. Shiue, S. Katzman, E.M. Munding, R. Shelansky, J.P. Donohue, and M. Ares. 2019. Rapidly evolving proto-introns in Saccharomyces genomes revealed by a hungry spliceosome. *PLoS Genet.* 15:e1008249. https://doi.org/10.1371/journal.pgen.1008249

Tam, J., and F.J. van Werven. 2020. Regulated repression governs the cell fate promoter controlling yeast meiosis. *Nat. Commun.* 11:2271. https://doi.org/10.1038/s41467-020-16107-w

Tsuchiya, D., Y. Yang, and S. Lacefield. 2014. Positive feedback of NDT80 expression ensures irreversible meiotic commitment in budding yeast. *PLoS Genet.* 10:e1004398. https://doi.org/10.1371/journal.pgen.1004398

Valášek, L., B. Szamecz, A.G. Hinnebusch, and K.H. Nielsen. 2007. In Vivo Stabilization of Preinitiation Complexes by Formaldehyde Cross-Linking. *Methods Enzymol.* 429:163–183. https://doi.org/10.1016/S0076-6879(07)29008-1

Varadi, M., S. Anyango, M. Deshpande, S. Nair, C. Natassia, G. Yordanova, D. Yuan, O. Stroe, G. Wood, A. Laydon, et al. 2022. AlphaFold protein structure database: Massively expanding the structural coverage of protein-sequence space with high-accuracy models. *Nucleic Acids Res.* 50:D439–D444. https://doi.org/10.1093/nar/gkab1061

Wagner, S., A. Herrmannová, V. Hronová, S. Gunišová, N.D. Sen, R.D. Hannan, A.G. Hinnebusch, N.E. Shirokikh, T. Preiss, and L.S. Valášek. 2020. Selective translation complex profiling reveals staged initiation and Co-translational assembly of initiation factor complexes. *Mol. Cell.* 79:546–560.e7. https://doi.org/10.1016/j.molcel.2020.06.004

van Werven, F.J., and A. Amon. 2011. Regulation of entry into gametogenesis. *Philos. Trans. R. Soc. Lond. B Biol. Sci.* 366:3521–3531. https://doi.org/10.1098/rstb.2011.0081

van Werven, F.J., G. Neuert, N. Hendrick, A. Lardenois, S. Buratowski, A. van Oudenaarden, M. Primig, and A. Amon. 2012. Transcription of two long noncoding RNAs mediates mating-type control of gametogenesis in budding yeast. *Cell*. 150:1170–1181. https://doi.org/10.1016/j.cell.2012.06.049

Williams, R.M., M. Primig, B.K. Washburn, E.A. Winzeler, M. Bellis, C. Sarrauste de Menthière, R.W. Davis, and R.E. Esposito. 2002. The Ume6 regulon coordinates metabolic and meiotic gene expression in yeast. *Proc. Natl. Acad. Sci. USA*. 99:13431–13436. https://doi.org/10.1073/pnas.202495299

Winstall, E., M. Sadowski, U. Kühn, E. Wahle, and A.B. Sachs. 2000. The Saccharomyces cerevisiae RNA-binding protein Rbp29 functions in cytoplasmic mRNA metabolism. *J. Biol. Chem.* 275:21817–21826. https://doi.org/10.1074/jbc.M002412200

Xu, L., M. Ajimura, R. Padmore, C. Klein, and N. Kleckner. 1995. NDT80, a meiosis-specific gene required for exit from pachytene in Saccharomyces cerevisiae. *Mol. Cell. Biol.* 15:6572–6581. https://doi.org/10.1128/MCB.15.12.6572

Yahya, G., A.P. Pérez, M.B. Mendoza, E. Parisi, D.F. Moreno, M.H. Artés, C. Gallego, and M. Aldea. 2021. Stress granules display bistable dynamics modulated by Cdk. *J. Cell Biol.* 220:e202005102. https://doi.org/10.1083/jcb.202005102

Yue, J.-X., J. Li, L. Aigrain, J. Hallin, K. Persson, K. Oliver, A. Bergström, P. Coupland, J. Warringer, M.C. Lagomarsino, et al. 2017. Contrasting evolutionary genome dynamics between domesticated and wild yeasts. *Nat. Genet.* 49:913–924. https://doi.org/10.1038/ng.3847

Zenklusen, D., D.R. Larson, and R.H. Singer. 2008. Single-RNA counting reveals alternative modes of gene expression in yeast. *Nat. Struct. Mol. Biol.* 15:1263–1271. https://doi.org/10.1038/nsmb.1514

JCB

Supplemental material

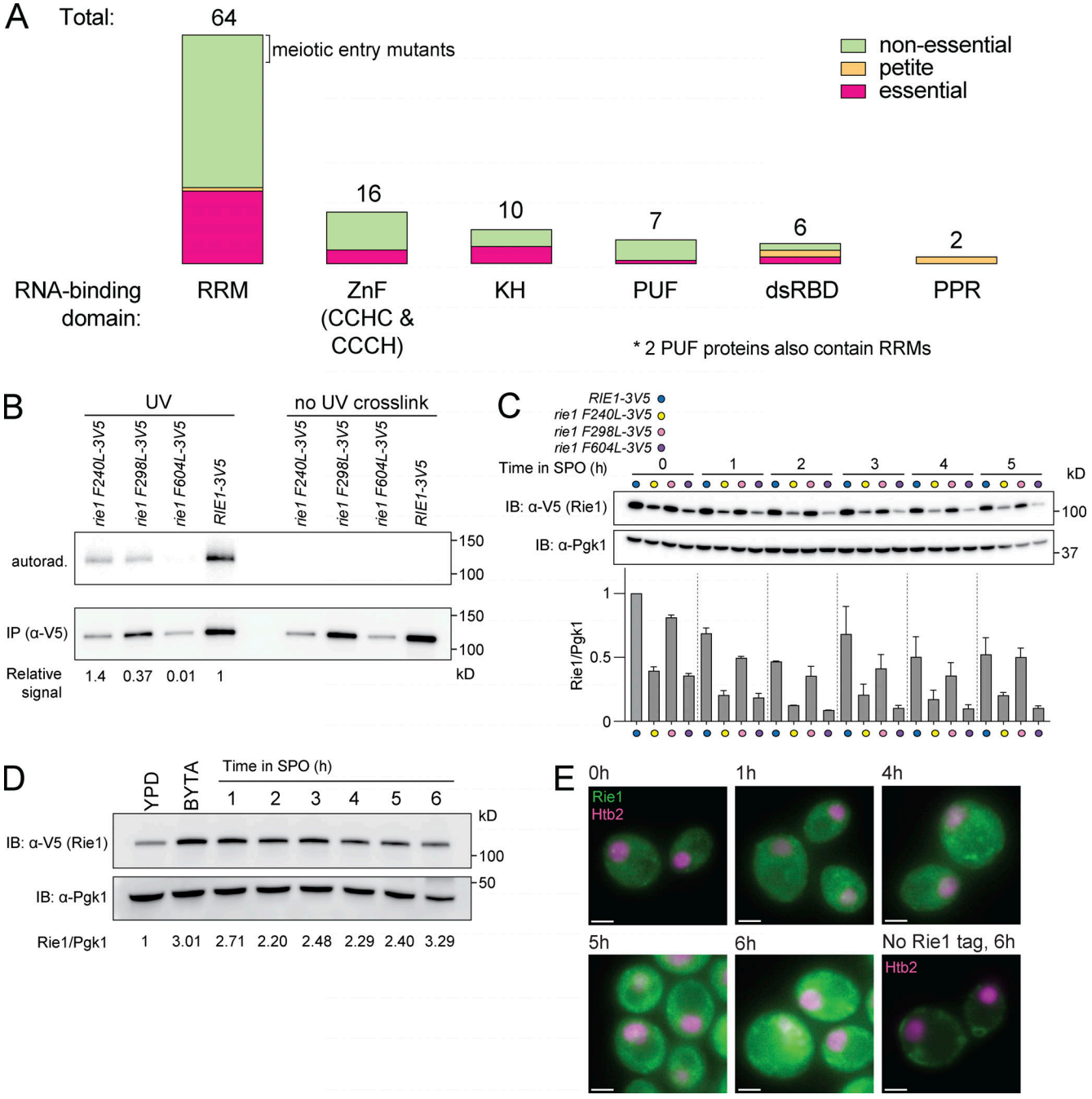

Figure S1. **Rie1 binds RNA and is involved in meiotic entry. (A)** Overview of protein characteristics of screened RBPs. For our forward screen for meiotic entry mutants, we considered 94 total genes encoding RBPs harboring at least one of the following domains: RRM, zinc finger (ZnF), K Homology domains (KH), Pumilio Family domains (PUF), double-stranded RNA binding domains (dsRBD), or pentatricopeptide repeat domains (PPR). Mutants in non-essential genes (green) were included in the screen. Mutants in essential genes (magenta) or petites (orange) were not included. **(B and C)** Strains harboring *RIE1-3V5* (B3114, blue), *rie1 F240L-3V5* (B2674, yellow), *rie1 F298L-3V5* (B2816, pink), or *rie1 604L-3V5* (B2680, purple) were induced to sporulate at 30°C. **(B)** Cells were collected either with or without UV crosslinking at 2 h in SPO. Samples were treated with DNAse and Rie1 was IPed under denaturing conditions, and bound RNA was assessed by a polynucleotide labeling assay. Shown are autoradiograms (top) indicating bound RNA and immunoblot (IB; bottom) indicating IPed Rie1. Quantifications of RNA-binding signal/IPed Rie1 protein are indicated below. **(C)** Protein levels of Rie1 and Pgk1 (loading) were determined by immunoblot at the indicated times. Quantification of Rie1 normalized to Pgk1 (three technical replicates) is shown below. **(D)** Strains harboring *RIE1-3V5* were grown in either YPD (log phase), BYTA (stationary phase), or induced to sporulate at 30°C. Samples were collected at the indicated times, and Rie1 and Pgk1 (loading) protein levels were determined by immunoblot. Quantifications of Rie1/Pgk1 compared with YPD (set at 1) are indicated below. Biological replicates = 3. **(E)** Strains harboring *HTB2-mCherry* and either *RIE1-ENVY* (B1554) or wild type *RIE1* (no tag control, B3680) were induced to sporulate at 30°C. Cells were collected at the indicated times and imaged by fluorescence microscopy. Rie1 is shown in green and Htb2 (histone indicating nucleus) is shown in magenta. Green signal in no tag likely represents autofluorescence from bud scars and mitochondria. Scale bar, 2 µm. Source data are available for this figure: SourceData FS1.

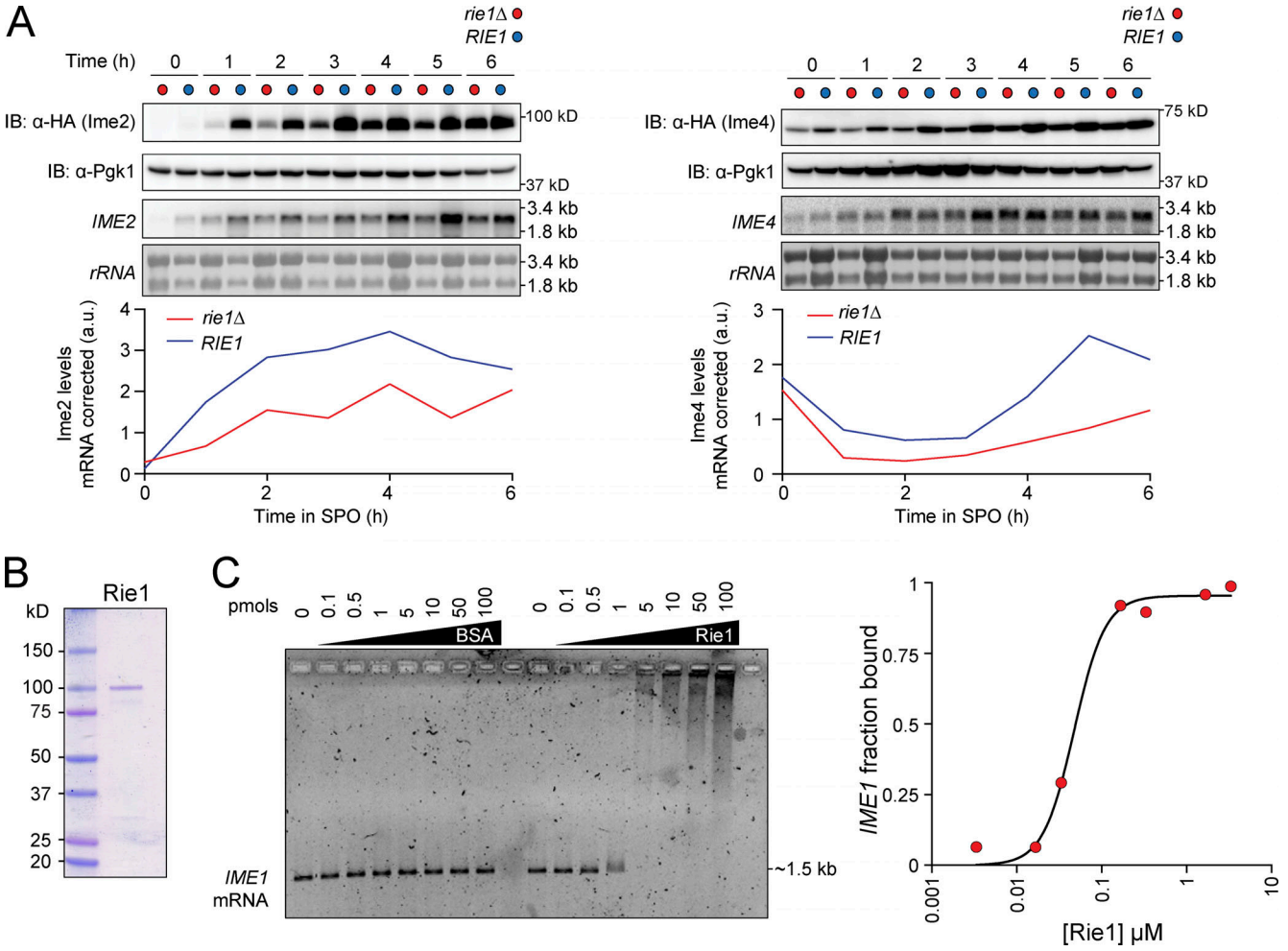

Figure S2. **Rie1 affects Ime2 and Ime4 levels and binds *IME1* mRNA. (A)** Strains harboring *IME2-3HA* and *rie1*Δ (B1701, red), or wild type *RIE1* (B1704, blue), or *IME4-3HA* and *rie1*Δ (B1656, red), or wild type *RIE1* (B1698, blue) were induced to sporulate at 30°C. Protein levels of Ime2, Ime4, and Pgk1 (loading) protein levels were determined by immunoblot (IB) and mRNA levels of *IME2*, *IME4*, and *rRNA* (loading) were determined by Northern blot. Quantifications of Ime2 and Ime4 protein levels (corrected for mRNA levels) are shown below. **(B and C)** Rie1 binds *IME1* mRNA. **(B)** Coomassie-stained SDS-PAGE of recombinant Rie1 purified from *E. coli*. **(C)** 5 pmol of in vitro transcribed *IME1* mRNA (including UTRs) was incubated with purified Rie1 or BSA (gradient from 100, 50, 10, 5, 1, 0.5, 0.1 pmol) for 45 min at 30°C. Samples were separated on agarose gels which were stained with SYBR Gold. Binding caused *IME1* mRNA to shift upwards. Percent bound *IME1* mRNA is plotted (y axis) vs. concentration of Rie1 (x axis). Source data are available for this figure: SourceData FS2.

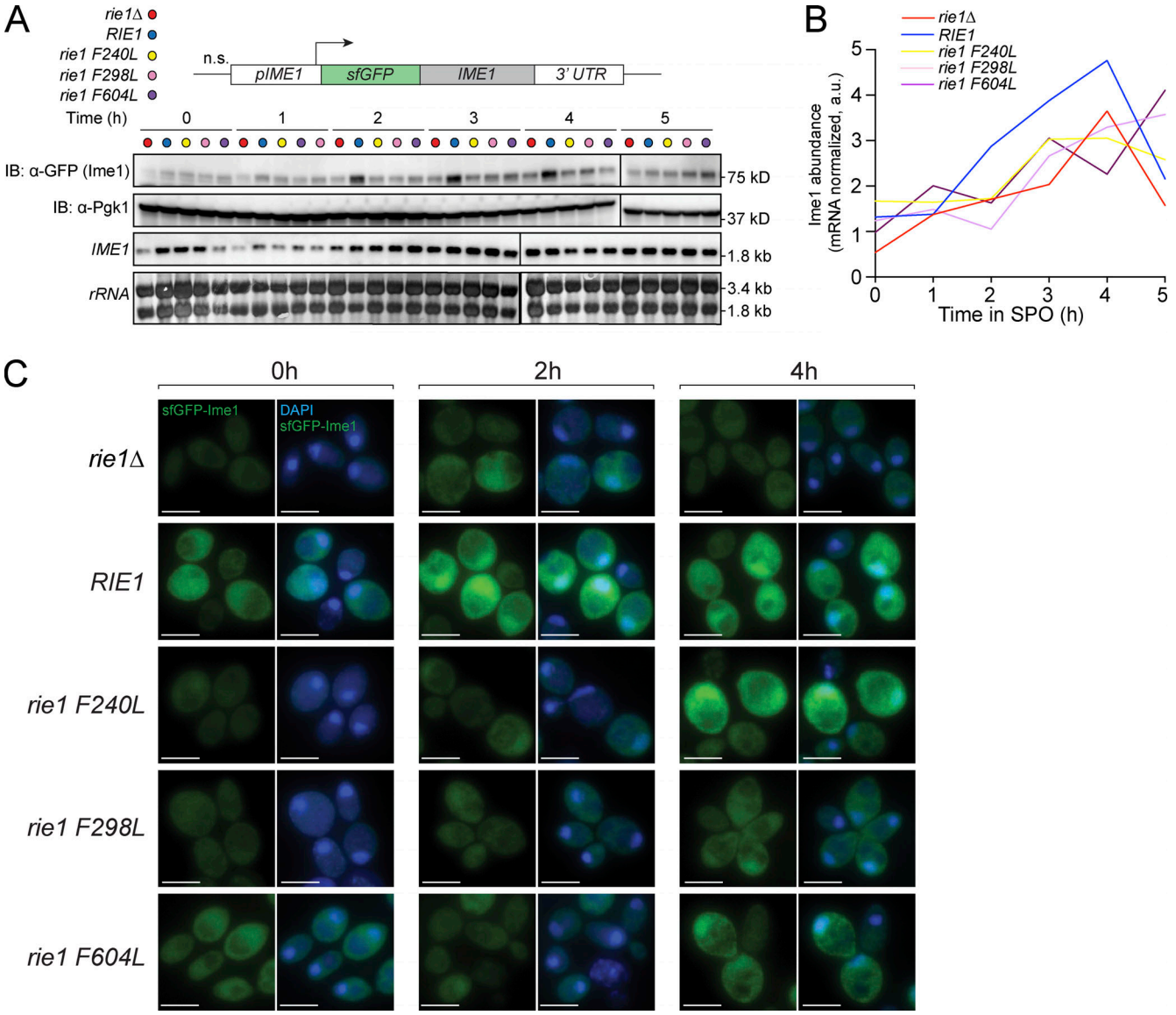

Figure S3. ***rie1* mutants accumulate lower levels of Ime1 protein. (A–C)** Strains harboring N-terminal sfGFP-tagged (*sfGFP-IME1*) and *rie1*Δ (B1653, red), wild type *RIE1* (B1662, blue), *rie1-F240L* (B2403, yellow), *rie1-F298L* (B2836, pink), or *rie1-F604L* (B2298, purple) were induced to sporulate at 30°C. **(A)** Protein levels of Ime1 and Pgk1 (loading) were determined by immunoblot (IB), and mRNA levels of *IME1* and *rRNA* (loading) were determined by Northern blot. **(B)** Quantifications of Ime1 protein corrected for mRNA levels are shown. Biological replicates = 5. **(C)** Examples of images quantified for Fig. 2 E. sfGFP-Ime1 is shown in green and DAPI is shown in blue. Scale bar, 5 µm. Source data are available for this figure: SourceData FS3.

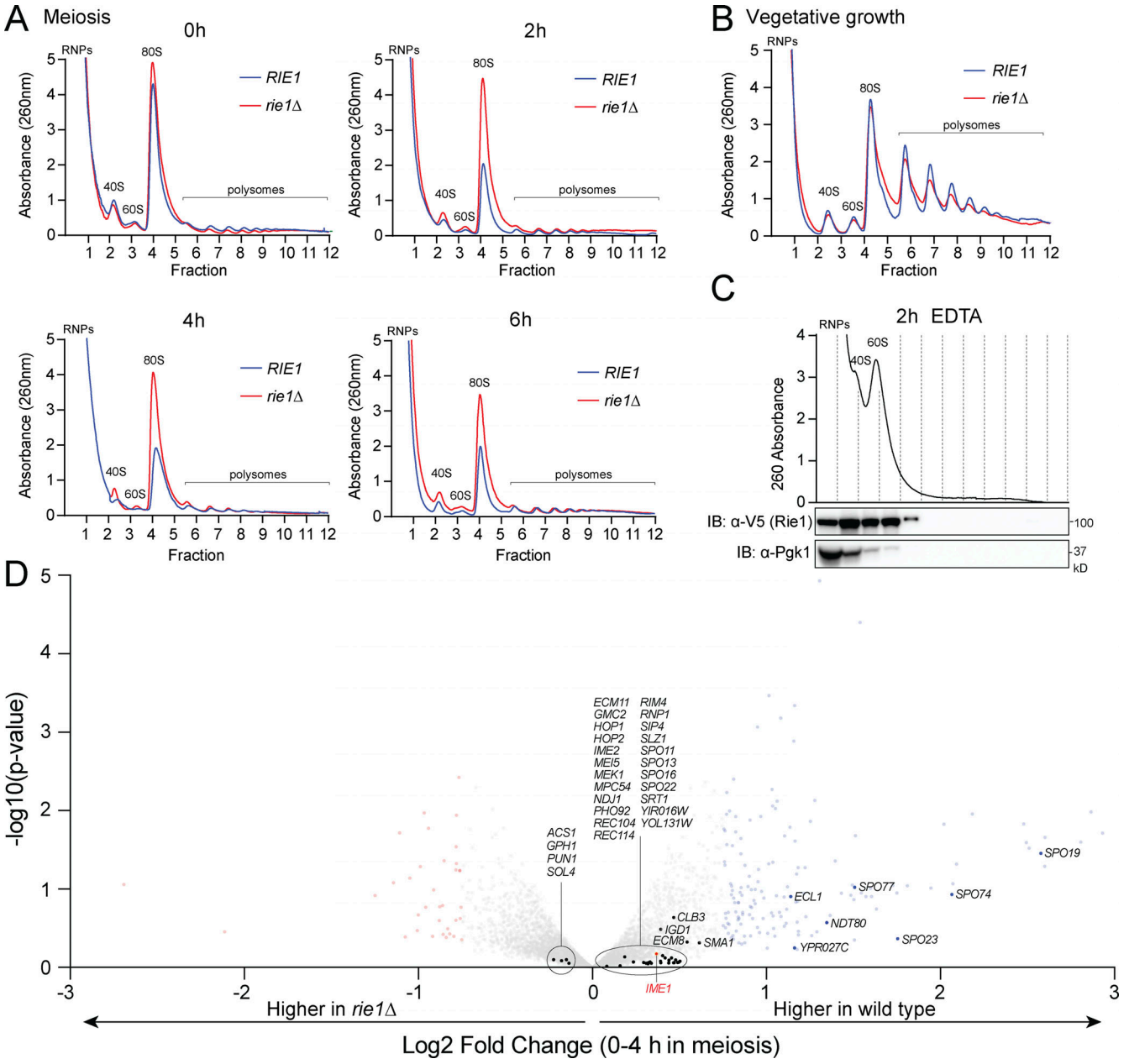

Figure S4. ***RIE1* affects global translation and transcript levels of the *UME6* regulon. (A–C)** Strains harboring *rie1*Δ (B1574, red) or wild type *RIE1* (B47, blue) were (A) induced to sporulate at 30°C or (B) grown to mid-log phase in rich medium (YPD) and samples were collected at the indicated times. Lysates were fractionated on 10–50% sucrose density gradients with continuous monitoring at 260 nm. Positions of the RNP, 40S, 60S, 80S, and polysomal ribosome peaks are indicated. **(C)** Lysates were treated with 25 mM EDTA to disrupt ribosomes prior to fractionation. Biological replicates = 2. IB, immunoblot. **(D)** Strains harboring *rie1*Δ (B1574, red) or wild type *RIE1* (B47) were induced to sporulate at 30°C and total RNA samples were collected at 0 and 4 h for RNA-seq analysis. Shown is a volcano plot of $\log_2$ fold change plotted against $-\log_{10}$ P value of RNA-seq reads for wild type and *rie1*Δ. Values represent a ratio of expression between the wild type and *rie1*Δ cells between the 0 and 4 h time points. The further right the value, the more enriched the mRNA in the wild type strain. Genes with a $\log_2$ fold change less than −0.75 are colored red and genes with a $\log_2$ fold change >0.75 are colored blue. Genes within the *UME6* regulon (putative *IME1* targets; from Williams et al., 2002) are labeled. *UME6* regulon genes (mean enrichment 0.561) are significantly enriched in wild type (two-tailed *t* test of 10,000 data randomizations: P value <0.0001). *IME1* mRNA is highlighted in red (fold change = 0.368; P value 0.67). Source data are available for this figure: SourceData FS4.

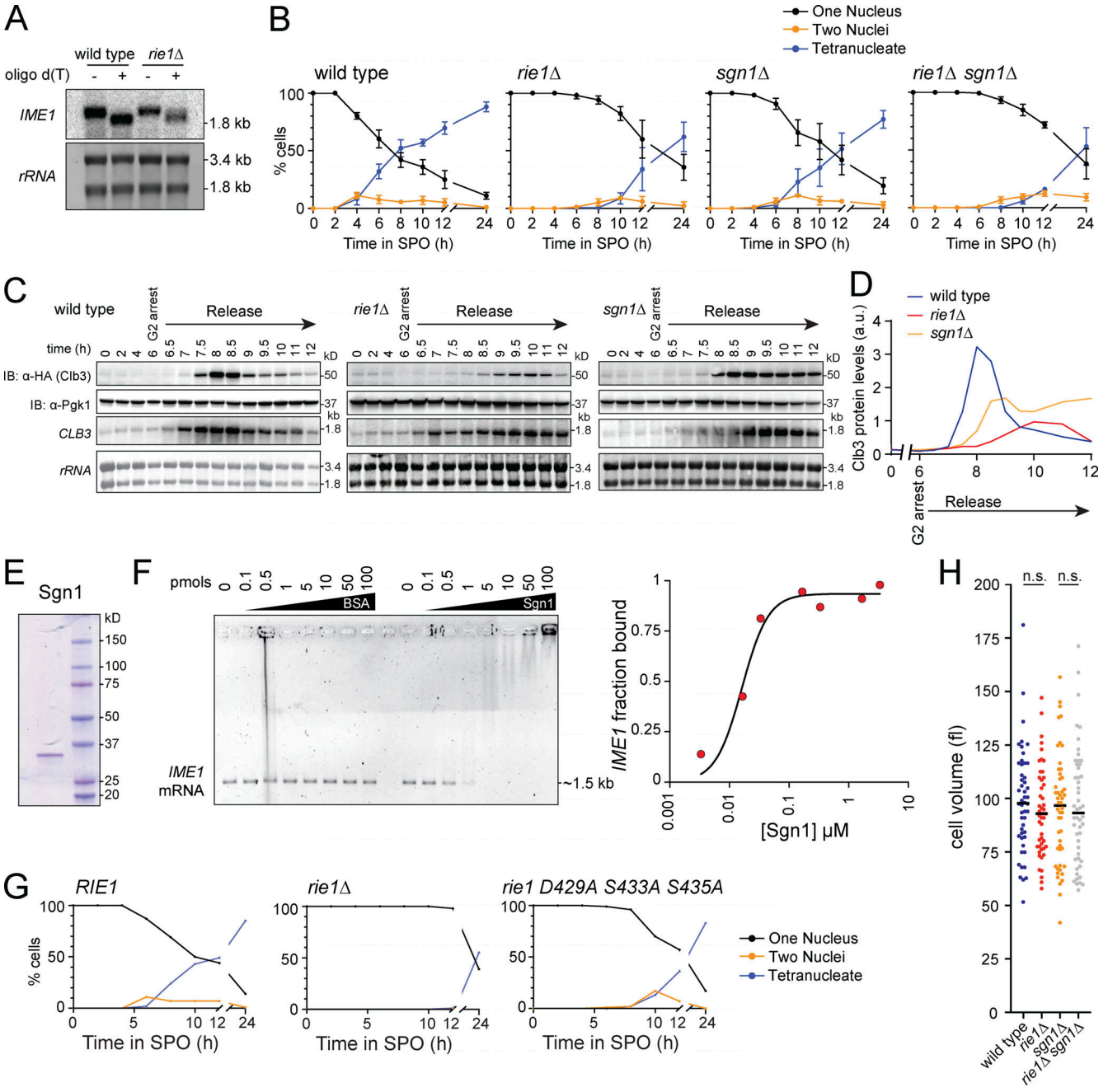

Figure S5. **Rie1 and Sgn1 work together to facilitate timely meiotic entry. (A)** Strains harboring *rie1*Δ (B1574) or wild type *RIE1* (B47) were induced to sporulate at 30°C and samples were collected at 2 h. *IME1* poly(A) tail length was assessed by oligo(dT) Northern blot assay. Differences in band sizes between samples with and without oligo(dT) indicate size of the poly(A) tail. Biological replicates = 2. **(B)** Strains harboring N-terminally tagged *sfGFP-IME1* and *rie1*Δ (B2430), wild type *RIE1* and *SGN1* (B2459), *sgn1*Δ (B3375), or *rie1*Δ *sgn1*Δ (B3378) were induced to sporulate at 30°C. Meiotic progression was determined by DAPI staining. Biological replicates = 3 and error bars indicate SEM. **(C and D)** Strains harboring *NDT80-IN*, *CLB3-3HA*, and either *rie1*Δ (B1418), *sgn1*Δ (B2606), or wild type *RIE1 SGN1* (B48) were induced to sporulate at 30°C. **(C)** Protein levels of Clb3 and Pgk1 (loading) protein levels were determined by immunoblot (IB), and mRNA levels of *CLB3* and *rRNA* (loading) were determined by Northern blot. Biological replicates = 2. **(D)** Clb3 quantification (loading corrected) are shown. **(E and F)** Sgn1 binds *IME1* mRNA. **(E)** Coomassie stained SDS-PAGE of recombinant Sgn1 purified from *E. coli*. **(F)** 5 pmol of in vitro transcribed *IME1* mRNA (including UTRs) was incubated with purified Sgn1 or BSA (gradient from 100, 50, 10, 5, 1, 0.5, 0.1 pmol) for 45 min at 30°C. Samples were separated on agarose gels that were stained with SYBR Gold. Binding caused *IME1* mRNA to shift upwards. Percent bound *IME1* mRNA is plotted (y axis) vs. concentration of Sgn1 (x axis). **(G)** Strains harboring N-terminal sfGFP-tagged (*sfGFP-IME1*) and *rie1*Δ (B1653, red), wild type *RIE1* (B1662, blue), *or rie1-D429A, S433A, S435A* (B3562, yellow) were induced to sporulate at 30°C. Meiotic progression was determined by DAPI. **(H)** Cell sizes of diploid wild type (B47, blue), *rie1*Δ (B1574, red), *sgn1*Δ (B3088, orange), and *rie1*Δ *sgn1*Δ (B3342, gray) strains were determined after overnight growth in BYTA (pre-meiotic) medium. Mean is indicated by a black bar and statistical significance ($P < 0.05$) was determined by student's *t* test.

Video 1. **Strains harboring fluorescently labeled tubulin (*pTUB1-GFP-TUB1*) and Spc42 (*SPC42-mCherry*) and wild type *RIE1* (B1451) were induced to sporulate at 30°C.** After 2.5 h of growth, the yeast cells were loaded onto a microfluidics chip (Cell Asic), points were established, and cells were imaged by time-lapse epifluorescence microscopy with frame capture every 7 min (shown here at six frames/second). Tubulin is shown in green and the spindle pole bodies in red.

Video 2. **Strains harboring fluorescently labeled tubulin (*pTUB1-GFP-TUB1*) and Spc42 (*SPC42-mCherry*) and *rie1*Δ (B1514) were induced to sporulate at 30°C.** After 2.5 h of growth, the yeast cells were loaded onto a microfluidics chip (Cell Asic), points were established, and cells were imaged by time-lapse epifluorescence microscopy with frame capture every 7 min (shown here at six frames/second). Tubulin is shown in green and the spindle pole bodies in red.

Provided online are four tables. Table S1 shows RBP screen strains and raw data. Table S2 shows the strains used in this study. Table S3 shows the reagent table. Table S4 shows RNA-seq raw data.